(12) INTERNATIONAL APPLICATION PUBLISHED UNDER THE PATENT COOPERATION TREATY (PCT)

(19) World Intellectual Property Organization
International Bureau

(43) International Publication Date
14 February 2013 (14.02.2013)

WIPO | PCT

(10) International Publication Number
WO 2013/023110 A2

(51) International Patent Classification:
B05D 1/02 (2006.01)

(21) International Application Number:
PCT/US2012/050223

(22) International Filing Date:
10 August 2012 (10.08.2012)

(25) Filing Language: English

(26) Publication Language: English

(30) Priority Data:
61/522,381 11 August 2011 (11.08.2011) US

(71) Applicant *(for all designated States except US)*: **THE TRUSTEES OF THE UNIVERSITY OF PENNSYLVANIA** [US/US]; 3160 Chestnut Street, Suite 200, Philadelphia, PA 19104 (US).

(72) Inventors; and
(75) Inventors/Applicants *(for US only)*: **YUNKER, Peter, J.** [US/US]; 3428 Sansom Street, Philadelphia, PA 19104 (US). **YODH, Arjun, G.** [US/US]; 231 Valley Road, Merion, PA 19066 (US).

(74) Agents: **RABINOWITZ, Aaron, B.** et al.; Woodcock Washburn LLP, Cira Centre, 12th Floor, 2929 Arch Street, Philadelphia, PA 19104-2891 (US).

(81) Designated States *(unless otherwise indicated, for every kind of national protection available)*: AE, AG, AL, AM, AO, AT, AU, AZ, BA, BB, BG, BH, BN, BR, BW, BY, BZ, CA, CH, CL, CN, CO, CR, CU, CZ, DE, DK, DM, DO, DZ, EC, EE, EG, ES, FI, GB, GD, GE, GH, GM, GT, HN, HR, HU, ID, IL, IN, IS, JP, KE, KG, KM, KN, KP, KR, KZ, LA, LC, LK, LR, LS, LT, LU, LY, MA, MD, ME, MG, MK, MN, MW, MX, MY, MZ, NA, NG, NI, NO, NZ, OM, PE, PG, PH, PL, PT, QA, RO, RS, RU, RW, SC, SD, SE, SG, SK, SL, SM, ST, SV, SY, TH, TJ, TM, TN, TR, TT, TZ, UA, UG, US, UZ, VC, VN, ZA, ZM, ZW.

(84) Designated States *(unless otherwise indicated, for every kind of regional protection available)*: ARIPO (BW, GH, GM, KE, LR, LS, MW, MZ, NA, RW, SD, SL, SZ, TZ, UG, ZM, ZW), Eurasian (AM, AZ, BY, KG, KZ, RU, TJ, TM), European (AL, AT, BE, BG, CH, CY, CZ, DE, DK, EE, ES, FI, FR, GB, GR, HR, HU, IE, IS, IT, LT, LU, LV, MC, MK, MT, NL, NO, PL, PT, RO, RS, SE, SI, SK, SM, TR), OAPI (BF, BJ, CF, CG, CI, CM, GA, GN, GQ, GW, ML, MR, NE, SN, TD, TG).

Declarations under Rule 4.17:

— *as to applicant's entitlement to apply for and be granted a patent (Rule 4.17(ii))*

— *as to the applicant's entitlement to claim the priority of the earlier application (Rule 4.17(iii))*

Published:

— *without international search report and to be republished upon receipt of that report (Rule 48.2(g))*

(54) **Title**: UNIFORM COATINGS PRODUCED BY SUSPENSIONS OF ANISOTROPIC PARTICLES

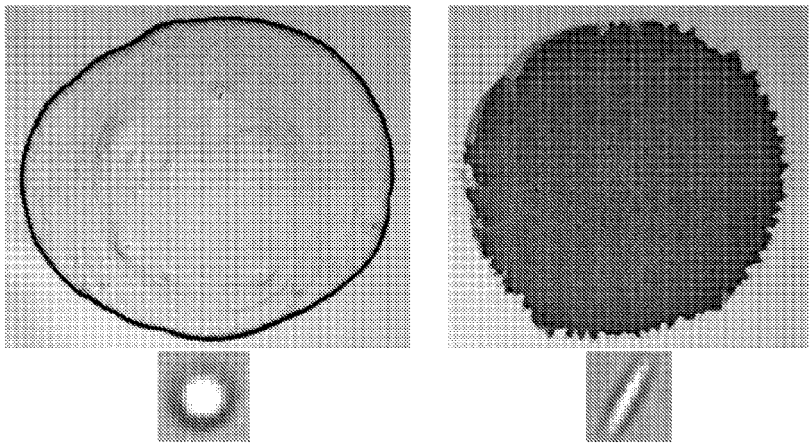

Figure 11

(57) **Abstract**: Provided are compositions that include anisotropic particles, which anisotropic particles enable the compositions to dry and leave behind a uniform distribution of particles instead of the so-called "coffee ring" of particles that typically characterizes dried droplets. Also provided are related methods of synthesizing and formulating such compositions.

WO 2013/023110 A2

UNIFORM COATINGS PRODUCED BY SUSPENSIONS OF ANISOTROPIC PARTICLES

RELATED APPLICATION

[0001] The present application claims the benefit of and priority to United States patent application 61/522,381, "Uniform Coatings Produced By Suspensions Of Anisotropic Particles," filed on August 11, 2011, the entirety of which is incorporated herein by reference for any and all purposes.

STATEMENT OF GOVERNMENT RIGHTS

[0002] This work was supported by National Science Foundation grants DMR-0804881 and DMR-0520020 and by National Aeronautics and Space Administration grant NNX08AO0G. The government has certain rights in this invention.

TECHNICAL FIELD

[0003] The present invention relates to the field of coating compositions, to the field of colloidal science, and to the field of soft condensed matter.

BACKGROUND

[0004] When a drop of liquid dries on a solid surface, its solute is quite often deposited in ring-like fashion. This phenomenon, known as the coffee ring effect, is familiar to anyone who has dried a drop of coffee. During the drying process, drop edges become pinned, and capillary flow outward from drop center brings suspended particles to the edge as evaporation proceeds. After evaporation, suspended particles are left highly concentrated along the original drop edge. The coffee ring effect is manifest in systems with diverse constituents ranging from large colloids to nanoparticles to individual molecules. In fact, notwithstanding the many practical applications for uniform coatings in printing, biology, and complex assembly, the ubiquitous nature of the effect has proven difficult to avoid. Accordingly, there is a need in the art for compositions and related methods capable of distributing suspended particles evenly along a substrate.

SUMMARY

[0005] In a first aspect, the present disclosure provides compositions, the compositions suitably including a fluid medium; a plurality of anisotropic bodies disposed within the fluid medium, at least some of the anisotropic bodies having an aspect ratio of major axis to minor axis of between about 1.0 and about 10,000, and at least some of the anisotropic bodies having at least one cross-sectional dimension in the range of from about 1 nm to about 500 micrometers.

[0006] The present disclosure also provides methods, the methods including dispersing a plurality of anisotropic bodies into a fluid medium, at least some of the anisotropic bodies having an aspect ratio of major axis to minor axis of greater than about 1.0, and the anisotropic bodies having at least one cross-sectional dimension in the range of between about 1.0 and about 10,000.

[0007] Also provided are methods for making uniform coatings, the methods including applying a plurality of droplets of a composition to a substrate, the composition comprising a fluid medium having a plurality of anisotropic bodies disposed within, at least some of the anisotropic bodies having an aspect ratio of major axis to minor axis of between about 1.0 and about 10,000.

[0008] Further disclosed are compositions, the compositions including a fluid medium; a plurality of anisotropic bodies disposed within the fluid medium, and at least some of the anisotropic bodies having hydrophobicities that differ from one another.

BRIEF DESCRIPTION OF THE DRAWINGS

[0009] The summary, as well as the following detailed description, is further understood when read in conjunction with the appended drawings. For the purpose of illustrating the invention, there are shown in the drawings exemplary embodiments of the invention; however, the invention is not limited to the specific methods, compositions, and devices disclosed. In addition, the drawings are not necessarily drawn to scale. In the drawings:

[0010] Figure 1 illustrates deposition of spheres and ellipsoids a,b. Image of the final distributions of ellipsoids (a) and spheres (b) after evaporation. c. Schematic diagram of the evaporation process depicting capillary flow induced by pinned edges. If the contact line were free to recede, the drop profile would be preserved during evaporation (dashed line). However, the contact line remains pinned, so the contact angle decreases (solid line). Thus, a capillary flow, from the drop's center to its edges, is induced to replenish fluid at the contact line. d.

Droplet-normalized particle number density, ρ/N, plotted as function of radial distance from center of drop for ellipsoids with various major-minor axis aspect ratios. e. The maximum local density, ρ_{Max}, normalized by the density in the middle of the drop, ρ_{Mid}, is plotted for all α. Lines guide the eye.

[0011] Figure 2 illustrates transportation of particles over time. a-h. Experimental snapshots at different times during the evaporation of a drop of spheres (a-d) and a drop of ellipsoids with aspect ratio $\alpha = 3.5$ (e-h). i. The areal particle density, ρR, located within 20 μm of the contact line (i.e., drop edge) as a function of time during evaporation. j-m. Images of the assembly of ellipsoids at the air-water interface over the same time intervals during evaporation. Loosely-packed structures form on the air-water interface, preventing ellipsoids from reaching the edge. The three phase contact line can be seen in the bottom left corner of these snapshots.

[0012] Figure 3 presents high magnification microscopy images of particles near the drop contact line. a-c. Images of a region within 40 μm of the drop contact line, taken at time $t/t_{Final} = 0.5$, for suspensions of spheres (a), ellipsoids ($\alpha = 3.5$) (b), and ellipsoids ($\alpha = 3.5$) mixed with surfactant (SDS) (0.2% by weight). Spheres pack closely at the contact line. Ellipsoids form loosely packed structures. Surfactant lowers the drop surface tension, making ellipsoids pack closely at the contact line. For a and b, pictures of the entire drop after evaporation are shown and the magnified region is indicated. d,e. Confocal projections of suspensions of ellipsoids ($\alpha = 2.5$) (d) and spheres (e) onto the z-r plane in cylindrical coordinates.

[0013] Figure 4 illustrates behavior of spheres, ellipsoids, and mixtures of spheres and ellipsoids in drying liquid drops. For all cartoons, the left and right panels are side views at early and late times, respectively, and the center panel is a top view showing particle trajectories linking those times. a-f. Cartoon depicting capillary flow that carries spheres (a-c) and ellipsoids (d-f) to the drop's edge. Spheres leave a ring-like formation, while ellipsoids form loosely-packed structures on the air-water interface. g. The deposition of mixtures of spheres and ellipsoids are characterized by the ratio $\rho' = \rho_{Max}/\rho_{Mid}$, where ρ_{Max} is the maximum local density and ρ_{Mid} is the density in the middle of the drop, as a function of ellipsoid volume fraction, ϕ_E. Two sizes of particles are studied: $d = 5.0$ μm (black squares), $d = 0.7$ μm (red circles), where d is the particle diameter. ρ' is normalized by ρ'_0, the value of ρ' when there are no ellipsoids present, i.e., $\phi_E = 0$. The coffee ring effect persists for mixtures of small spheres and ellipsoids,

but is destroyed for mixtures of large spheres and ellipsoids. Error bars represent the uncertainty that results from finite bin sizes. h-j. Cartoon depicting capillary flow that carries suspensions of spheres and ellipsoids to the drop's edge.

[0014] Figure 5 presents the mass, m, of drops of different suspensions plotted versus time, t, for evaporating drops. Suspensions of spheres ($\alpha = 1.0$ black squares) and ellipsoids ($\alpha = 3.5$ open red circles) are shown, as well as a drop of water absent colloids (blue triangles).

[0015] Figure 6 presents the radius, R, of drops of different suspensions plotted versus time, t, for evaporating drops. Suspensions of spheres ($\alpha = 1.0$ black line) and ellipsoids ($\alpha = 3.5$ red line) are shown. To facilitate comparisons, the time is normalized by the time evaporation ends (t_{Final}), and R is normalized by the value of R at $t = 0$ s.

[0016] Figure 7 presents the Boussinesq number, B0, for ellipsoids with $\alpha = 3.5$ plotted versus time, t, normalized by the time evaporation finishes, t_F. The red line is the best exponential fit.

[0017] Figure 8 presents a. the final distribution of core-shell polystyrene-NIPA spheres. These hydrophilic particles exhibit the coffee ring effect. b. The final distribution of core-shell polystyrene-NIPA ellipsoids. These particles, which are both anisotropic and hydrophilic do not exhibit the coffee ring effect.

[0018] Figure 9 presents the three-phase contact angle, θ_C plotted versus aspect ratio, a. Inset: Image of a 100 μl drop of a suspension containing ellipsoids with $\alpha = 3.5$

[0019] Figure 10 presents a. the final distribution of ellipsoids, evaporated from a suspension with initial volume fraction $\phi = 0.20$. b. The final distribution of spheres, evaporated from a suspension with initial volume fraction $\phi = 0.20$.

[0020] Figure 11 depicts the dispersion of particles in a standard droplet (left) and in a droplet according to the present disclosure (right);

[0021] Figure 12 (from http://www.mulliganscoffeebeans.com/) depicts an exemplary coffee ring effect from droplet drying in a standard suspension without anisotropic particles;

[0022] Figure 13 (from Deegan et al., *Nature* 389, 827–829 (1997)) depicts a cutaway view of the evaporation process in a coffee ring system;

[0023] Figure 14 depicts a cutaway view of the evaporation process in a coffee ring system;

[0024] Figure 15 depicts spheres deposited in a ring arrangement from evaporating a solution free of anisotropic particles;

[0025] Figure 16 depicts an exemplary method for fabricating ellipsoids from polystyrene microspheres;

[0026] Figure 17 depicts the effect of an ellipsoid particle on a fluid interface;

[0027] Figure 18 depicts ellipsoids residing at an air/fluid interface;

[0028] Figure 19 illustrates that adding surfactant to an exemplary composition according to the present disclosure can restore the so-called coffee ring effect;

[0029] Figure 20 illustrates the situation of confined evaporation of a droplet containing anisotropic particles of various aspect ratios (α);

[0030] Figure 21 illustrates the effect of anisotropic particles (ellipsoids) on the coffee ring effect in a sessile drop – the left-hand of the figure illustrates evaporation behavior of a droplet that contains spheres, and the right-hand of the figure illustrates evaporation behavior of a droplet that contains ellipsoidal anisotropic particles;

[0031] Figure 22 depicts the physical configuration of a droplet confined between two opposing plates (right-hand side of figure), where confinement acts to impair the ability of ellipsoids (or other particles) from reaching the air-fluid interface;

[0032] Figure 23 illustrates that in the evaporative drying of a sessile drop, ellipsoids are distributed more evenly than spheres;

[0033] Figure 24 illustrates that in a droplet that contains spherical particles and ellipsoids (anisotropic particles), the spheres distribute more evenly upon evaporation than they do in a droplet that contains only spherical particles.

[0034] Figure 25 presents a. Image of a pinned region of the air-water interface (α = 1.0). When the pinned section does not ``snap" off, it leaves behind a channel. b. At a later time (~100 seconds after (c)), the channel extends, and more particles flow into it, producing a very heterogeneous deposition. c. Image of the final deposition of particles with major-minor diameter

aspect ratio $\alpha = 1.0$. The box indicates the deposit left behind by the event depicted in (a) and (b). d. Image of a colloidal monolayer near the three phase contact line in a drop containing ellipsoids ($\alpha = 3.5$). The three phase contact line is labeled with a dashed line on the left side of the image. Particles are adsorbed on the air-water interface, forming a monolayer, as evidenced by the fact that particles become more out of focus, from left to right, as the air-water interface curves. A cartoon below shows a side view of the experimental image. e. The fraction of area covered by particles, f, for suspensions of 200 nm diameter spheres doped with different amounts of ellipsoids, represented by the ellipsoid volume fraction, φE.

[0035] Figure 26 illustrates the bending rigidity, κ, of the particle coated air-water interface plotted as a function of particle aspect ratio, α

[0036] Figure 27 presents (a) Cartoon depicting droplet evaporating in a confined geometry. The particle-populated air-water interface and three-phase contact lines are labeled. (b), (c) Examples of buckling events for confined drops containing anisotropic particles with $\alpha = 1.2$ and 1.5 [(b),(c) respectively]. (d) Rim width, d (solid line), is defined here in a magnified image of a buckled region as the interface full-width 25 μm from the vertex of the bent air-water interface (see dashed line). (e) d is plotted versus the square root of the drop radius, r. (f) Ratio of the bending rigidity, κ, to the Young's modulus, E, is plotted versus α. (g) κ versus E, where E comes from previously reported measurements and calculations. The line represents the best power law fit. (h) κ versus α; and

[0037] Figure 28 presents images of the final deposition of particles with major-minor diameter aspect ratio $\alpha = 1.0$; 1.2; 1.5; 2.5; 3.5 [(a)–(e), respectively]. (f) The area fraction covered by particles after evaporation is complete, f, for suspensions of particles as a function of their aspect ratio α.

DETAILED DESCRIPTION OF ILLUSTRATIVE EMBODIMENTS

[0038] The present invention may be understood more readily by reference to the following detailed description taken in connection with the accompanying figures and examples, which form a part of this disclosure. It is to be understood that this invention is not limited to the specific devices, methods, applications, conditions or parameters described and/or shown herein, and that the terminology used herein is for the purpose of describing particular embodiments by way of example only and is not intended to be limiting of the claimed invention. Also, as used in

the specification including the appended claims, the singular forms "a," "an," and "the" include the plural, and reference to a particular numerical value includes at least that particular value, unless the context clearly dictates otherwise. The term "plurality", as used herein, means more than one. When a range of values is expressed, another embodiment includes from the one particular value and/or to the other particular value. Similarly, when values are expressed as approximations, by use of the antecedent "about," it will be understood that the particular value forms another embodiment. All ranges are inclusive and combinable.

[0039] It is to be appreciated that certain features of the invention which are, for clarity, described herein in the context of separate embodiments, may also be provided in combination in a single embodiment. Conversely, various features of the invention that are, for brevity, described in the context of a single embodiment, may also be provided separately or in any subcombination. Further, reference to values stated in ranges include each and every value within that range. Any and all documents cited in this application are incorporated herein by reference in their entireties.

[0040] In a first aspect, the present disclosure provides methods of creating an essentially uniform particle deposition. These methods include applying, to a portion of a substrate, a composition that suitably includes a fluid medium and a plurality of anisotropic bodies disposed within the fluid medium. At least some of the anisotropic bodies suitably have an aspect ratio of major axis to minor axis of between about 1.0 and about 10,000. At least some of the anisotropic bodies also suitably have at least one cross-sectional dimension in the range of from about 1 nm to about 500 micrometers. The methods also include evaporating at least a portion of the fluid medium.

[0041] The anisotropic bodies suitably have at least one cross-sectional dimension (e.g., diameter, length) that is in the nanometer range, although a nanometer-scale cross-sectional dimension is not a requirement. Cross-sectional dimensions in the range of from about 5 nm to about 100 micrometers, or from about 10 nm to about 50 micrometers, or even from about 100 nm to about 5 micrometers are all considered suitable.

[0042] As one example, Pf1 viruses are considered suitable bodies. Such viruses may have a minor axis length of ~6 nm. Anisotropic particles of virtually any size may be used; suitable particles may be chosen such that gravity does not force them to sediment before they

reach the air-water interface. Carbon nanotubes are considered suitable bodies, particularly where the carbon nanotubes are stabilized (e.g., with charge, or even sterically stabilized).

[0043] It is particularly suitable for the anisotropic bodies to be about as dense as the fluid medium (in this case the particles are about 5% more dense than the fluid). Less dense bodies are also suitable, as this will simply make the bodies reach the interface faster. If the anisotropic particles are denser than the fluid medium, this effect can still work. Even if the particles are pushed to the edge at the bottom of the drop, they will adsorb onto the interface and then become nearly evenly dispersed.

[0044] The bodies are suitably stabilized in some manner; charge stabilization and steric stabilization are both suitable ways to stabilize particles. A user may also use a surfactant to stabilize particles; surfactants that do not greatly reduce surface tension are considered especially suitable.

[0045] In the exemplary case of anisotropic polystyrene particles, the particles may begin as charge-stabilized spheres. These polystyrene spheres have charge groups (e.g., sulfate, carboxyl, amidine) on their surfaces. After the spherical particles are stretched (described elsewhere herein) to achieve an ellipsoidal shape, the groups remain on the particle surface, and the particles remain charge stabilized. Additional detail is shown in Figure 16.

[0046] Aspect ratios of 1.5, 2.5, and 3.5 are all suitable. There is essentially no practical upper limit to the aspect ratio. Actin filaments may be used as anisotropic bodies, and such filaments have aspect ratios in the range of from about 2000 to about 3000. At least some of the anisotropic bodies may have an aspect ratio of major axis to minor axis of between about 10 and about 10,000, 1,000, or even between from about 100 and about 500.

[0047] Virtually any anisotropic shape that creates an interparticle attraction at the air-fluid interface is suitable. Some examples include ellipsoids, barbells, rods, doublets (two spheres that are connected), triplets (three connected spheres), branched particles (e.g., tripods), cubic particles, tetrahedra, as well as chemically heterogeneous particles (Janus particles). The population of anisotropic bodies may be polydisperse in terms of size, aspect ratio, material composition, size, shape, or in some other aspect, such as hydrophobicity.

[0048] In a given composition, the anisotropic bodies may represent represents a volume fraction of from about 0.0001 to about 0.2 of the composition, or even a volume fraction

of from about 0.001 to about 0.02 of the composition. A volume fraction of 0.3, 0.4, or 0.5 is also suitable.

[0049] Virtually any fluid medium may be used in the disclosed compositions. Water, alcohol, and other fluids are all considered suitable. Oils and hydrocarbons are also suitable fluids. A user may select a fluid based on the fluid's non-reactivity with the anisotropic bodies or other components of the composition.

[0050] The disclosed compositions may also include a population of spherical or non-anisotropic bodies. As described elsewhere herein, the anisotropic bodies may act to restrain the movement of the spherical bodies within the composition (e.g., during evaporation). In this way, the anisotropic bodies act to effect essentially even or even uniform dispersion of the spherical bodies within a quantity (e.g., a droplet) of the composition. At least some of the essentially spherical bodies suitably have a diameter that is greater than the minor axis of the plurality of anisotropic bodies. Without being bound to any single theory of operation, it is believed that such spherical bodies, by virtue of their dimensions, become entrapped in the network of anisotropic bodies and cannot travel outwards to the edge of an evaporating droplet of fluid. A spherical body can be of virtually any material; it may be a polymer, a mineral, a metal, a biological entity (e.g., cell, tissue, organelle, organ, or any part thereof), and the like. The spherical body may include a strand of DNA, or even comprise an individual molecule. Exemplary molecules include biological molecules, chemical molecules and the like.

[0051] Anisotropic bodies can likewise be composed of virtually any material. Bio-materials (such as FD viruses, PF1 viruses, actin filaments, bacteria, and the like), core-shell particles (e.g., core-shell polystyrene-PNIPAm particles), metal particles, silicon particles, and the like are all suitable anisotropic bodies. Bodies that are denser than the fluid medium are suitably of a comparatively small size so as to reduce or even avoid sedimentation. Core-shell particles are considered especially suitable, as the core may be of a comparatively inexpensive material, and the shell may be used to carry some active material (e.g., DNA or other biologic).

[0052] In some embodiments, the composition may include one or more pigments. The pigment may be included in an anisotropic body, as a sphere, or even in the fluid itself. Pigmented compositions are considered especially useful, as the composition enables uniform distribution of the pigment throughout a droplet during evaporation of the fluid medium.

[0053] The pigment may be present as a body or other particle. Such pigment bodies suitably have a major axis larger than the minor axis of the plurality of anisotropic bodies. In this way, the pigment bodies are restrained by the network of anisotropic bodies, and do not migrate to the edge of a drop of the composition. It should be understood that the compositions may include anisotropic and isotropic (e.g., spherical) bodies.

[0054] The compositions may also contain a mono- or polydisperse mixture of anisotropic, spherical, or both bodies, as explained elsewhere herein. For example, a composition might include anisotropic bodies having a ratio of major to minor axis of 2:1 as well as bodies having a major:minor axis ratio of 5:1. The composition may include bodies that are thermoplastic (e.g., polyethylene) in nature, which bodies in turn allow for uniform dispersion of the compositions bodies across a surface, after which the bodies may be thermally processed to form an essentially uniform coating.

[0055] The compositions may also be formulated such that some of the bodies disposed within the composition are sacrificial, such that the composition may be disposed on a substrate so as to achieve a uniform disposition of the composition bodies, after which some of the bodies are eliminated (e.g., via chemical treatment, by heat, by application of radiation, or by other techniques known in the art). In this way, a user may achieve a final coating that include fewer than all of the bodies present in the composition initially.

[0056] The present disclosure also provides methods. These methods suitably include dispersing a plurality of anisotropic bodies into a fluid medium, at least some of the anisotropic bodies having an aspect ratio of major axis to minor axis of greater than about 1.0, and the bodies having at least one cross-sectional dimension in the range of between about 1.0 nm and about 500 micrometers.

[0057] Suitable fluids and bodies are described elsewhere herein. The methods may also include dispersing spheres or other bodies having a major axis that is greater than the minor axis of the anisotropic bodies. The user may also disperse a pigment into the composition; suitable pigments are also described elsewhere herein.

[0058] Additionally disclosed methods include applying a plurality of droplets of a composition to a substrate, the composition comprising a fluid medium having a plurality of anisotropic bodies disposed within, at least some of the anisotropic bodies having an aspect ratio of major axis to minor axis of between about 1.0 and about 10,000.

[0059] The methods may further include removing at least a portion of the fluid medium following application of the plurality of droplets. This may be effected, e.g., in printing applications, where the user (using, e.g., an inkjet or other printer) may apply droplets of the composition to a substrate and then evaporate the fluid medium so as to leave behind the bodies in the fluid. In some embodiments, the anisotropic bodies may be selectively removed (e.g., by application of heat, chemical reagent, or both) so as to leave behind the spheres, pigment, or other constituents in the composition.

[0060] A user may also apply thermal energy or a chemical reagent to one or more droplets so as to bond two or more anisotropic bodies. In this way, the user may create a network of anisotropic bodies on a substrate after the fluid medium has been removed. The user may also apply heat or a chemical reagent to bind spheres or pigment bodies to one another, or even to bind an anisotropic body to a sphere or pigment. The heat or reagent may bond or fuse multiple particles to one another so as to leave behind a network of particles. The heat or reagent may also be used to melt a previously-formed network so as to liberate a reagent that is disposed within some portion of the network particles.

[0061] In this way, a user may apply the disclosed compositions to achieve a uniform dispersion of particles, and then evaporate the fluid, which evaporation leaves behind an even dispersion of particles. The user may then heat (or otherwise process) the particles so as to fuse the particles together (e.g., in the case of a thermoplastic particle) into a network. By virtue of being formed from an even distribution of constituent particles, the resultant network will itself be even.

[0062] The disclosed compositions have many applications. For example, many coatings and paints contain two solvents, water and something that evaporates slower than water (e.g., an oil). After the water evaporates away, the coating particles are left in the slowly evaporating oil, where they form a film. If the slowly evaporating oil were removed, the coating would exhibit the coffee ring effect. The disclosed compositions enable the user to eliminate the second solvent, making the process faster and more economical

[0063] The coatings created by the disclosed compositions are uniform and are also essentially monolayers in form. This is useful in the field of electronics for heat transfer, as thinner, nmore uniform coatings (e.g., conductive metals) allow electronics to dissipate heat

more efficiently. Further, this can be useful in the miniaturization of technology, as a thin but effective coating allows more space for other components.

[0064] Alternatively, if insulating materials are used in the disclosed compositions, the uniformity of the resultant coating can be reduced, with only a small change to optical properties. This is in turn useful for windows or other applications where optical properties are a consideration.

[0065] The compositions are also useful in packaging applications. A monolayer of material may act to keep air-tight seals shut, but the monolayer also will not impair the user's ability to open a container.

[0066] In addition, monolayers generally naturally require less material to create. To create a seal with polystyrene spheres, a larger number of particles would be required to compensate for the coffee ring effect. Similarly, inkjet printer inks cost about $3 per milliliter, despite the fact that 95% of the ink is water. Thus, reducing the amount of particulate material (i.e., pigment, spheres) in the ink can effect substantial savings.

[0067] The disclosed compositions and methods are also useful in complex assembly. Complicated materials can be assembled one monoloayer at a time. One potential application of this type is photonics or creation of metamaterials. Many such materials can be built out of thin uniform layers of different compositions. For example, a user may construct a device by depositing a quantity of material according to the present disclosure onto a substrate (or position a quantity of the material between two surfaces) and evaporating (or allowing to evaporate) the fluid medium. It should be understood that the surfaces may be solid (e.g., substrates), but may also be fluids. As an example, an amount of a composition may be positioned between layers of two other fluids. This will leave behind an essentially uniform dispersion of particles. The user may then place a second quantity of material atop the same location and allow this second quantity to dry, so as to leave a second layer of uniformly-distributed particles atop the first layer. In this way, a user may build up multiple layers of material. The layers of material may be of the same particles or of different particles.

[0068] In alternative embodiments, the user may select the particles of the composition to give rise to selective layers. For exampler, the user may employ a composition that includes anisotropic particles that may be chemically degraded and spherical particles that are chemically resistant. In such a case, the user may apply the composition and evaporate the fluid medium,

leaving behind an essentially uniform distribution of anisotropic particles and spheres. The user may then remove the anisotropic particles (e.g., by application of a suitable chemical agent that selectively removes the anisotropic particles but does not affect the spheres). The user may then leave behind the uniform distribution of spheres or, depending on the user's needs and the characteristics of the spheres, apply heat (e.g., in the case of thermoplastic spheres) to bond the spheres to one another to create a network of fused particles. Alternatively, a chemical agent (e.g., a solvent or adhesive) may be used to network deposited particles. In this manner, a user may formulate compositions that result in a coating of fewer than all of the different kinds of particles or bodies in the fluid composition. The user may, of course, build up structures or regions by depositing multiple particle populations atop one another.

[0069] A user may also add anisotropic particles (in a volume fraction of from 0.00001 to about 20, 30 or even 50%) to an existing suspension or colloid containing spherical particles. The addition of the anisotropic particles will confer on the composition the ability to produce essentially uniform (or at least more uniform) particle depositions upon evaporation of the fluid medium. In this way, the user may modify or even improve the performance of existing compositions, such as paints, inks, and other coating compositions.

[0070] The disclosed compositions and methods are also useful in biotechnology applications. One such application is genotyping. In genotyping, different complementary strands of DNA are attached to a substrate at known locations. The DNA being investigated is then washed over the substrate. The sequences present in the investigated DNA are then identified based on where it attaches to the substrate.

[0071] However, uneven coatings of complementary strands of DNA can make the process less efficient. Solutions to this problem typically rely on complex multi-stage processes and additional chemicals that may have unintended secondary effects. Instead, if the complementary strands of DNA are attached to anisotropic particles, the DNA strands will be deposited uniformly and in a bio-friendly aqueous environment.

[0072] The present compositions may also be applied to liquid bandages. Wounds can be covered with a solution including anisotropic particles. After evaporation, the coating left behind will prevent contaminants from entering the wound, as the coating will be dense and uniformly distributed across the wound. The coating may also be breathable, helping the wound

to heal. The coating also would allow the patient to be more mobile, as a monolayer is not very restricting.

[0073] A user may use heat or reduced humidity to effect evaporation of the fluid medium. Ambient conditions may also be useful to evaporating the fluid medium.

EXEMPLARY EMBODIMENTS

[0074] Here is shown that suspended particle shape may effect coatings and can be used to eliminate the coffee ring effect. Ellipsoidal particles deposit uniformly during evaporation. The anisotropic particles significantly deform interfaces, producing strong interparticle capillary interactions. Thus, after the ellipsoids are carried to the air-water interface by the same outward flow that causes the coffee ring effect for spheres, strong long-ranged interfacial attractions towards other ellipsoids lead to the formation of loosely-packed quasi-static or arrested structures on the air-water interface. These structures prevent the suspended particles from reaching the drop edge and ensure uniform deposition. Under appropriate conditions, suspensions of spheres mixed with a small number of ellipsoids also produce uniform deposition.

[0075] A drop of evaporating water is a complex, difficult-to-control, non-equilibrium system. Along with capillary flow, the evaporating drop features a spherical-cap-shaped air-water interface and Marangoni flows induced by small temperature differences between the top of the drop and the contact line. Attempts to reverse or ameliorate the coffee ring effect have thus far focused on manipulating capillary flows. In this disclosure it is shown that uniform coatings during drying can be obtained by changing particle shape. The uniform deposition of ellipsoids after evaporation (Fig. 1a) is readily apparent, and it stands in stark contrast to the uneven "coffee ring" deposition of spheres (Fig. 1b) in the same solvent, with the same chemical composition, and experiencing the same capillary flows (Fig. 1c).

[0076] Much of the physics of the coffee ring effect has been demonstrated with micron-sized polystyrene particles . This disclosure uses such particles and modifies their shape. The disclosed experiments employ water drops containing a suspension of micron-sized polystyrene spheres (Invitrogen) stretched asymmetrically to different aspect ratios. Similar results were obtained for hydrophilic ellipsoids and other anisotropic particles (see Figure 8). Drops were evaporated on glass slides (Fisher Scientific) and study suspensions containing

particles of the same composition, but with different major-minor diameter aspect ratio (a), including spheres ($\alpha = 1.0$), slightly deformed spheres ($\alpha = 1.05, 1.1, 1.2, 1.5$), and ellipsoids ($\alpha = 2.5, 3.5$); volume fractions ($\phi$) were studied that vary from $\phi = 10^{-4}$ to 0.2.

[0077] During the drying process, the droplet contact line remains pinned in all suspensions, and fluid (carrying particles) flows outward from drop center to replenish the edges. Spherical articles are efficiently transported to the edge, either in the bulk or along the air-water interface, leaving a ring after evaporation is complete. Anisotropic particles ($a > 1.0$), however, are only transported toward the edge until they reach the air-water interface. For example, once at the air-water interface, ellipsoids experience strong long-ranged attractions to other ellipsoids, leading to the formation of loosely-packed quasi-static or arrested structures at the interface. On the interface, the interparticle attraction between anisotropic particles is more than two orders of magnitude stronger than the attraction between spheres. Thus, anisotropic particles in these "open" structures are comparatively strongly bound to each other and to the interface, so the energy cost of deforming, moving, or breaking up these clusters is large. As a result, ellipsoid mobility is markedly reduced, and they resist the radially outward flow. Thus, when evaporation is complete, anisotropic particles are much more uniformly deposited on the glass surface than spheres. While spheres also adsorb onto the interface during evaporation, they do not significantly deform the interface. Therefore, the radially outward fluid flow continues to push them to the drop's edge. Fig. 1 shows the final deposition, after evaporation on glass slides at 23° C, of two particle suspensions ($\phi = 0.005$, 1 μl) with different aspect ratios. Spherical particles are primarily deposited at the original perimeter of the droplet (Fig. 1 b). Ellipsoidal particles are distributed much more uniformly (Fig. 1 a).

[0078] To quantify the behavior shown qualitatively in Fig. 1a and b, one may determine the areal number fraction ($\rho(r)$) of particles deposited as a function of radial distance from the drop center, normalized by the number of particles (N) (Fig. 1d). For spheres ($\alpha = 1.0$), ρ/N is ~70 times larger at $r/R \approx 1$ than in the middle of the drop. Conversely, the density profile of ellipsoidal particles is fairly uniform as a function of r/R. As aspect ratio is increased from unity, the peak at large r/R decreases. A coffee ring effect persists for particles only marginally distorted from their original spherical shape ($\alpha = 1.05$ and 1.1), but particles slightly more anisotropic ($\alpha = 1.2$) are deposited uniformly. This behavior is summarized by calculating

$\rho MAX/\rho MID$ (Fig. 1e), where ρ_{MAX} is the maximum value of ρ (typically located at $r/R \approx 1$) and ρ_{MID} is the average value of ρ in the middle of the drop ($r/R < 0.25$).

[0079] Quantification of the spatio-temporal evaporation profile of the suspensions provides a first step toward understanding why ellipsoids are deposited uniformly. One may measure drop mass of different suspensions during evaporation (Fig. 5). The drop mass decreases linearly in time, and the mass rate-of-change of 10.0 μg/s is the same for drops of sphere suspension, drops of ellipsoid suspension, and pure water drops.

[0080] To confirm that the contact line remains pinned until the final stage of evaporation, one may measure the drop radius during evaporation by video microscopy. Using these data, the time at which evaporation finishes, t_{Final}, is readily identified as the time when the drop radius shrinks to zero. One finds that the radius decreases by less than 10% until $t = 0.8\ t_{Final}$; i.e., the contact line is pinned for the vast majority of the evaporation time period in all samples. For suspensions of ellipsoids, the contact line becomes partially depinned around $t = 0.7\ t_{Final}$, but does not become completely depinned until $t = 0.8\ t_{Final}$. The experiments thus demonstrate that despite similar contact line behavior, capillary flow, and evaporation rates, the deposition of spheres and ellipsoids differs significantly.

[0081] Experimental image snapshots clearly reveal that while spheres are carried to the drop's edges (Fig. 2a-d), ellipsoids are carried there to far lesser degree (Fig. 2e-h). one may measure the average areal particle density close to the contact line, $\rho_R = \int_{r=R-2s_{ph}}^{r=R} \rho(r)dr$ as a function of time (Fig. 2i), and thereby demonstrated that ellipsoid density grows at a slower rate than sphere density.

[0082] Images of particles near the drop's contact line (Fig. 2j-m) reveal that unlike spheres, which are carried from the bulk all the way to the contact line (Fig. 4a-c), most ellipsoids adhere to the loosely-packed structures at the air-water interface before they reach the contact line (Fig. 4d-f). This capillary attraction has been characterized in prior experiments as long-ranged and very strong. The loosely-packed configurations formed by ellipsoids on the interface are structurally similar to those seen in previous experiments of ellipsoids at flat air-water and water-oil interfaces. They produce a surface viscosity that is much larger than the bulk viscosity, facilitating ellipsoid resistance to radially outward flows (see Supplemental Information). Spheres also adsorb onto the interface during evaporation. However, spheres do

not strongly deform the interface and they experience a much weaker interparticle attraction than ellipsoids; thus, radially outward fluid flows push spheres to the drop's edge.

[0083] Snapshots of the region within 40 μm of the drop contact line confirm that while spheres pack closely at the edge (Fig. 3a), ellipsoids form loosely packed structures (Fig. 3b), which prevent particles from reaching the contact line. Particles with $\alpha = 1.2$ and 1.5 pack at higher area fractions than ellipsoids with $\alpha > 1.5$, resulting in larger values of $\rho_{MAX/\rho MID}$ for $\alpha =$ 1.2 and 1.5 and producing the small peak in $\rho(r)$ at $r/R = 0.7$ for $\alpha = 1.2$. The structures on the air-water interface appear to be locally arrested or "jammed", i.e., particles do not rearrange. Once an ellipsoid joins a collective structure, its position relative to other ellipsoids changes by less than 20 nm and the structure only rearranges when new particles become attached to the interface. In order to quantify the ability of interfacial aggregates of ellipsoids to resist bulk flow, one may calculate the Boussinesq number for the experimental system (see additional disclosure, elsewhere herein), i.e., the ratio of the surface drag to bulk drag for ellipsoids with $\alpha= 3.5$. The calculated Boussinesq number is greater than 1, and grows exponentially with time (see Fig. 7). Shear stress grows linearly with particle velocity, but elastic modulus grows exponentially with ellipsoid area fraction; and dominates the ratio. As might be anticipated, the Boussinesq number for spheres was much smaller than for ellipsoids, i.e., it is less than 1.

[0084] To confirm that deformations of the interface are responsible for the uniform deposition of ellipsoids, one may add a small amount of surfactant (e.g., sodium dodecyl sulfate, SDS, 0.2% by weight) to a suspension of ellipsoids with $\alpha = 3.5$. Surfactant lowers the surface tension of the drop, thus making interfacial deformations less energetically costly and shorter-range. This restores the coffee ring effect; ellipsoids pack closely at the contact line (Fig. 3c), in a manner similar to spheres. The ellipsoids no longer strongly deform the air-water interface and their interactions with other ellipsoids are correspondingly reduced; as a result, they move more easily along and on-and-off the interface and are able to pack close to the contact line. (Without added surfactant, ellipsoids increase the air-water surface tension, as evidenced by an increase in contact angle from ~15° for spheres to ~35° for ellipsoids with $\alpha=3.5$ (Fig. 9).) This is also shown by Figure 19, which figure illustrates that addition of a surfactant to a fluid containing anisotropic particles will restore the coffee ring effect.

[0085] Direct evidence was obtained that the ellipsoids sit at the air-water interface, using three-dimensional confocal microscopy. Confocal snapshots, projected onto a side view of

the drop, clearly confirm that ellipsoids sit at the air-water interface (Fig. 3d), while spheres do not and are carried all the way to the contact line (Fig. 3e).

[0086] One may show that the addition of small numbers of ellipsoids to sphere suspensions can also destroy the coffee ring effect. If spheres are smaller than ellipsoids, then the coffee ring persists; if spheres are larger than the ellipsoid minor axis, then the coffee ring is destroyed. To observe this effect one may evaporate drops of suspensions containing both ellipsoids and spheres.

[0087] An exemplary suspension contains ellipsoids with $\alpha = 3.5$, stretched from particles of diameter $d = 1.3\ \mu m$, and spheres suspended at a volume fraction $\phi = 0.02$. Evaporative deposits are characterized as a function of ellipsoid volume fraction ϕE via $\rho'(\phi E) = \rho Max/\rho Mid$ (Fig. 4g). First, one may evaporate suspensions containing smaller spheres with d = 0.7 μm along with the ellipsoids at volume fractions ranging from $\phi_E = 0$ to $1.5\ 10^{-4}$. After evaporation, the spheres displayed a clear coffee ring, and this coffee ring persists even if more ellipsoids are added to the initial suspension (Fig. 4g). The coffee ring effect is uninhibited because spheres that are smaller than the ellipsoids are easily able to move under or through the loosely packed particle structures and reach the drop's edge (Fig. 4h-j).

[0088] If, instead, one evaporates suspensions containing larger spheres with $d = 5.0\ \mu m$, along with the same ellipsoids at the same volume fractions utilized previously, then different phenomena emerge. When the ellipsoid volume fraction is very small ($\phi_E \leq 2.5\ 10^{-5}$), the suspensions still exhibit a clear coffee ring effect. However, at larger ϕ_E, the coffee ring is diminished, and it eventually disappears at sufficiently large ϕ_E, i.e., $\phi_E \approx 1.5\ 10^{-4}$ (Fig. 4g). In this case, the larger spheres adsorb onto the air-water interface farther from the drop edge than do the ellipsoids. In the absence of ellipsoids, the spherical particles form closely-packed aggregates, but in the presence of ellipsoids they instead join the loosely-packed aggregates, eliminating the coffee ring effect (Fig. 4h-j). Thus, uniform depositions can potentially be made with existing suspensions, simply by adding ellipsoids.

[0089] A similar effect is seen when ellipsoids are added to suspensions of spheres which are then evaporated in confinement. However, in confinement the size of the sphere has no effect. Suspensions of 200 nm spheres ($\alpha = 1.0$) with $\varphi = 0.02$ were combined with suspensions containing micron-sized ellipsoids ($\alpha = 3.5$) at lower volume fractions, $\varphi = 0$ to 4.0E-3. The resulting colloidal drops were evaporated in the same confined geometries. The

addition of a very small number of ellipsoids has no effect on the deposition of spheres ($\varphi \leq$ 1.7E-3). Surprisingly, the addition of a larger, but still small, number of ellipsoids leads to a uniform deposition of both ellipsoids and spheres, i.e., f~0.8, despite the fact that spheres outnumber ellipsoids by a significant factor (10E3 - 10E4) (Fig. 25e). Apparently, spheres do not prevent ellipsoids from adsorbing on the air-water interface, and the CMM bending rigidity is dominated by the presence of ellipsoids. Thus, the membrane still resists bending around pinning sites. This behavior in confined geometries is different than that of sessile drops wherein it was discovered that if the spheres are larger than the ellipsoids, then the spheres are distributed uniformly after drying, but if the spheres are smaller than the ellipsoids, then they exhibit the coffee ring effect. From this perspective, it is somewhat surprising that small spheres are deposited uniformly from droplets doped with small numbers of ellipsoids and confined between glass plates.

[0090] Accordingly, without being bound to any particular theory, the addition of ellipsoids or other anisotropic particles to a confined solution will produce a uniform deposit when the ellipsoids (or other anisotropic particles) can adsorb on the air-water interface. This technique is effective for micron sized colloids, nanometer sized colloids and macromolecules, and also for individual molecules. It should be understood that the presence of anisotropic (e.g., ellipsoid) particles is effective in forming uniform deposits in sessile (open) and in confined drops (confined drops may be confined between surfaces that are fluid or solid).

[0091] The ability to deposit particles uniformly is desirable in many applications. Unfortunately, most proposed methods for avoiding the coffee ring effect require long multistage processes, which can be costly in manufacturing or require use of organic solvents which are sometimes flammable and toxic. Here it is shown that by exploiting a particle's shape, a uniform deposit can be easily derived from an evaporating a solution (e.g., an aqueous solution) that contains the particles. Other methods of inducing strong capillary interactions, e.g., surface roughness, may also produce uniform deposits.

[0092] Figure 26 shows the bending rigidity, κ, of the particle coated air-water interface plotted as a function of particle aspect ratio, α. As α increases, κ increases by almost two orders of magnitude. Without being bound to any single theory, it is more energetically costly to bend an interface covered with ellipsoids than to bend an interface covered with spheres.

[0093] The uniform deposition of ellipsoids in confined drops can be explained by measuring the bending rigidity of the particle laden air-water interface as a function of particle shape. Ellipsoids produce a large bending modulus, while spheres produce a small bending modulus. Both spheres and ellipsoids attach to the air-water interface. Ellipsoids deform the air-water interface, creating an effective elastic membrane with a high bending rigidity. When enough ellipsoids are present, pinning and bending the interface becomes energetically costly and the spheres (and ellipsoids) are deposited as the interface recedes.

[0094] Methods

[0095] Synthesis of Ellipsoids

[0096] To create ellipsoidal particles, 1.3 μm diameter polystyrene particles are suspended in a polyvinyl alcohol (PVA) gel and are heated above the polystyrene melting point (100° C), but below the PVA melting point (180°C). Polystyrene melts in the process, but the PVA gel only softens. The PVA gel is then pulled so that the spherical cavities containing liquid polystyrene are stretched into ellipsoidal cavities. When the PVA gel cools, polystyrene solidifies in the distorted cavities and becomes frozen into an ellipsoidal shape. The hardened gel dissolves in water, and the PVA is removed via centrifugation (see Supplementary Information). Each iteration of this process creates ~109 ellipsoidal particles in ~50 μl suspensions. The particles are charge-stabilized, and the resultant suspensions are surfactant-free. Snapshots of experimental particles are shown in the insets of Fig. 1a, b. The aspect ratio polydispersity is 10%. To ensure the preparation process does not affect particle deposition, spheres undergo the same procedure, absent stretching.

[0097] Confocal Snapshots

[0098] Confocal snapshots are shown in Fig. 3d and e. By integrating the brightness of each pixel over a period of 0.05 seconds, only particles that are roughly stationary during this time period appear in the images. Snapshots are then projected onto a side-view of the drop.

SUPPLEMENTAL DISCLOSURE

[0099] To quantify the behavior shown qualitatively in Fig. 1a and b, one may determine the areal number fraction of particles deposited as a function of radial distance from the drop center (Fig. 1d). Specifically, image analysis enables counting of the number of particles, N_r, in an area set by the annulus bounded by radial distances r and $r + \delta r$ from the

original drop center; here δr is ~8 μm. The areal particle density $\rho(r) = N_r/A$, with $A = \pi((r + \delta r)^2 - r^2)$. To further eliminate small sample-to-sample particle density differences, one may normalize ρ by the total number of particles in the drop, N, and thereby report $\rho(r)/N$ as a function of r/R, where R is the drop radius. Dilute suspensions ($\phi = 0.005$) are utilized to improve image quantification. For spheres ($\alpha = 1.0$), ρ/N is ~70 times larger at $r/R \approx 1$ than in the middle of the drop. Conversely, the density profile of ellipsoidal particles is fairly uniform as a function of r/R, though there is a slight increase at large r/R. As aspect ratio is increased in between these extremes, the peak at large r/R decreases. Specifically, a clear coffee ring effect persists for particles only marginally distorted from their original spherical shape ($\alpha = 1.05$ and 1.1), but particles that are slightly more anisotropic ($\alpha = 1.2$) are deposited uniformly.

[0100] To further quantify the peaked deposition of spheres and the more uniform deposition of ellipsoids, one may calculate and plot ρ_{MAX}/ρ_{MID} (Fig. 1e), where ρ_{MAX} is the maximum value of ρ (typically located at $r/R \approx 1$) and ρ_{MID} is the average value of ρ in the middle of the drop ($r/R < 0.25$). For spheres, $\rho_{MAX}/\rho_{MID} \approx 70$. As aspect ratio increases slightly ($\alpha = 1.05$ and 1.1) ρ_{MAX}/ρ_{MID} decreases to ~38 and 13, respectively. For ellipsoids, ρ_{MAX}/ρ_{MID} is more than ten times smaller. A second, relatively small aspect-ratio deposition effect is also observed for the ellipsoids; as a increases above 1.2, ρ_{MAX}/ρ_{MID} decreases slightly. Note, the value of ρ_{MAX}/ρ_{MID} was observed to be largely independent of initial volume fraction, i.e., ρ_{MAX}/ρ_{MID} fluctuated by approximately ±10% as volume fraction changed between $\phi = 10^{-4}$ and 0.2.

[0101] Mass

[0102] Quantification of the spatio-temporal evaporation profile of the suspensions provides a first step towards understanding why ellipsoids are deposited uniformly. To this end, one may measure drop mass of different suspensions (20 μl in volume, 6.0 mm in radius, ϕ = 0.005), during evaporation (Fig. 5). (Large drops were utilized in this experiment to improve the accuracy of the evaporation rate measurement.) The drop mass decreases linearly in time, and the mass rate-of-change of 10.0 μg/s is the same for drops of sphere suspension, drops of ellipsoid suspension, and for drops of water absent colloid. The evaporation behavior is also consistent with steady-state vapour-diffusion-limited evaporation of a spherical-cap-shaped drop with a pinned contact line.

[0103] Radius

[0104] To confirm that the contact line remains pinned until the final stage of evaporation, one may measure the radius of the 1 μl drops (ϕ = 0.005) during evaporation by video microscopy (Fig. 6). Using this data, the time at which evaporation finishes, *tFinal*, is readily identified as the time when the drop radius shrinks to zero. The radius decreases by less than 10% until t = 0.8 t_{Final}; i.e., the contact line is pinned for the vast majority of the evaporation time period in all samples. For suspensions of ellipsoids, the contact line becomes partially depinned around t = 0.7 t_{Final}, but does not become completely depinned until t = 0.8 t_{Final}. Thus, despite similar contact line behavior, capillary flow, and evaporation rates, the deposition of spheres and ellipsoids differs significantly.

[0105] Area fraction at edge

[0106] For spheres, ρR increases linearly until evaporation is complete, with a slope of 0.54 s^{-1}. The areal density of ellipsoids near the contact line, however, stops growing at t/t_{Final} = 0.75; for $t/t_{Final} < 0.75$, ρR increases with a slope of 0.15 s^{-1}, less than 1/3 the slope for spheres despite similar evaporation rates, capillary flows, and contact line behaviors.

[0107] Final Stage of Evaporation

[0108] Finally, during the last stages of evaporation, surface flows are observed to carry ellipsoids on the air-water interface from the drop edges back towards the drop center. This process often leaves a region near the contact line mostly void (see experimental snapshots Fig. 2g and h). The voided region decreases as ϕ increases (the aforementioned bump in $\rho(r)$ for α = 1.2 is located at the edge of this voided region).

[0109] Interfacial Resistance to Bulk Flow

[0110] In order to quantify the ability of interfacial aggregates of ellipsoids to resist bulk flow, one calculates the Boussinesq Number for ellipsoids with α = 3.5. The Boussinesq number, B_0, is the ratio of the surface drag to the bulk drag : $B_0 = \frac{G'}{\tau L}$ where r is shear stress from bulk flow, G' is the elastic modulus of the interfacial layer, and L is the probed lengthscale. B_0 will vary spatially with the local number of ellipsoids on the air-water interface, so one may focus here on a region within 40 μm of the contact line. One may first calculate B_0 at an early time (t = 0.1 t_F). The shear stress, calculated from the particle velocity and drop height is $r \approx 3\ 10^{-4}$ Pa. About 40% of the surface is covered with ellipsoids. Using the surface coverage area

fraction, one obtains the modulus of the interfacial monolayer (G' $\approx 10^{-3}$ N/m) from previous experimental studies. The probed length scale, L, is at most 0.01 m. Thus, at $t = 0.1t_F$, $B_0 \sim 300$. This calculation is performed at different times during evaporation, until the aggregate of ellipsoids begins flowing towards the drop center (Fig. 7). The Boussinesq number grows exponentially with time: $B_0 \propto exp(\frac{t}{0.12t_F})$ This is expected as r grows linearly with particle velocity, which increases by a factor of ~2 during evaporation. However, G' grows exponentially with the ellipsoidal area fraction, and area fraction increases by a factor of 3. Thus, the exponential growth of G' dominates this calculation. For spheres, $B_0 < 1$.

[0111] Final Distribution of Other Anisotropic Particles

[0112] Three additional types of anisotropic particles are analyzed. First, one may obtain suspensions of spherical and ellipsoidal polystyrene-PNIPAm core-shell particles, i.e., polystyrene particles coated with PNIPAm. These suspensions were evaporated at 23°C; at this temperature, PNIPAm is hydrophilic. The core-shell spheres exhibit the coffee ring effect (Fig. 8). Despite their hydrophilicity, the core-shell ellipsoids are deposited evenly. In fact, they form the same aggregates on the drop surface that polystyrene ellipsoids that are not coated with PNIPAm do (Fig. 8).

[0113] Also explored were suspensions of actin filaments and Pf1 viruses. In these suspensions, the contact line becomes depinned at very early times. To prevent this, one may add a small amount of 50 nm diameter florescent polystyrene spheres (~1% by weight), which pin the contact line until the final stage of evaporation ($t > 0.8\ t_F$), and thus exhibit the coffee ring effect. Both the actin filaments and Pf1 viruses are then deposited uniformly. Note, the mean major axis length for Pf1 viruses is ~2 μm and the mean major axis length for actin filaments is ~20 μm.

[0114] Three-Phase Contact Angle

[0115] The three-phase contact angle, θ_C, was measured by placing a large drop (100 μl) on a glass slide. Then, a side-view picture was taken, allowing the contact angle to be measured (Fig. 9). Spheres do not modify the contact angle. However, as a increases, θ_C increases as well.

[0116] Removal of PVA

[0117] After stretching ellipsoids, PVA is removed by centrifuging and washing each sample with water at least 10 times. A separate set of experiments were performed investigating the effects PVA has on evaporating drops, in order to ensure the PVA was not affecting the results. In these experiments, one may control the PVA weight percent. If a sample contains more than 0.5% PVA by weight, then the contact line depins after the drop is placed on a glass slide. However, in samples with less than 0.5% PVA by weight, contact line behavior is identical to the contact line behavior in drops without PVA. To confirm that small amounts of PVA do not affect the deposition of spheres, one may add PVA (0.45% by weight) to a suspension of spheres. During evaporation, the contact line remains pinned, and the spheres exhibit the coffee ring effect. Further, when ellipsoids are diluted by a factor of 100, and thus the PVA weight percent is decreased by a factor of 100 (to an absolute maximum of 0.05%), the deposition of the spatially uniform deposition of ellipsoids persists.

[0118] High Volume Fractions

[0119] When the volume fraction is large enough, the drop surface may become saturated with particles, such that the remaining particles in the bulk are transported to the drop edge. However, at high volume fractions it becomes difficult to quantify the local particle density. Thus, while the particles that cannot attach to the interface are likely transported to the drop edge, it is difficult to demonstrate that this occurs. A drop of ellipsoids ($\alpha = 3.5$) suspended at volume fraction $\phi = 0.20$ was evaporated. An experimental snapshot after evaporation is complete demonstrates that overall the coffee ring effect is destroyed, but the local density cannot be extracted (Fig. 10). An image of the final distribution of spheres evaporated from a suspension with initial packing fraction $\phi = 0.20$ is included for comparison.

[0120] Further disclosure is presented in Figures 11-19. Figure 11 illustrates (left-hand side) a traditional coffee ring pattern that results from evaporation of a fluid droplet that contains some particulates. The right side of Figure 11 illustrates a uniform distribution of particles that results from evaporation of a droplet according to the present disclosure, which droplet includes anisotropic particles.

[0121] Figure 12 provides a more detailed representation of the so-called coffee ring effect. As shown in this figure, after a droplet of a liquid containing particulates (e.g., coffee) evaporates, a ring-shaped deposit of particulate is left behind. This may be explained as set forth in Figure 13, which depicts the evaporation of a droplet; while evaporation occurs across the

surface of the drop, the edges of the droplet will evaporate first. The contact line (Figure 14) is pinned, so fluid flows to the contact line to replenish the fluid. Colloids (or other particles) are carried with the fluid to the edge of the droplet. The result of such a mechanism is shown in Figure 15, which figure shows the characteristic ring-link deposition of spheres that present in a fluid droplet that has evaporated. As shown in Figure 1, the inclusion of anisotropic particles in such a fluid droplet can prevent the formation of such a coffee ring pattern and instead promote uniform or even distribution of particles when the fluid evaporates, as shown in the right-side of Figure 1.

[0122] Figure 16 depicts an exemplary method of forming anisotropic (ellipsoidal) particles from spheres. As shown in the figure, polystyrene spheres (PS) are suspended in a matrix of polyvinyl alcohol (PVA). Heat is applied to the composition, which heat liquefies the PS spheres while leaving the PVA solid. The composition is stretched, which stretching elongates the cavities in which the PS spheres resided, and the liquid PS conforms to the newly-stretched cavities. The composition is then cooled, and the PS solidifies into ellipsoidal bodies. The ellipsoidal bodies may have an aspect ratio of greater than 1; as shown in the figure, the process may be used to form bodies having an aspect ratio of about 3.

[0123] The effect of anisotropic (ellipsoidal) bodies is shown in Figure 17. That figure shows that ellipsoids pull the air-fluid interface "down" at the ellipsoids' tips and pull the interface "up" along the sides or length of the ellipsoids. There is a quadripolar symmetry to this configuration, and the ellipsoids' effect on the interface gives rise to a long-range attractive force between ellipsoids. This attraction in turn forms a network of anisotropic particles (and can also include spheres or other non-anisotropic particles), which network acts to reduce the movement of particles in a fluid when a droplet of the fluid evaporates. This network can be characterized as a loosely-packed structure at the air-fluid interface. Figure 18 illustrates a comparison between the positions of spheres (top) and ellipsoids (bottom) in a drop, as shown in cross-section. As shown in the figure, the ellipsoids form a loosely-packed structure at the fluid-air interface, whereas the spheres are (top) essentially concentrated at the edge of the drop.

[0124] Figures 20-24 further illustrate the effect of the presence of anisotropic particles in a droplet. Figure 20 illustrates the evaporation of a confined droplet containing anisotropic particles of various aspect ratios (α). As shown in Figure 20, the greater the aspect ratio of the anisotropic particles, the more even the distribution of particles following evaporation. This

demonstrates that the advantages of the present disclosure are not confined to standard droplets having an upper surface open to the environment.

[0125] Further illustration of this effect is shown in Figure 21. In Figure 21, the left-hand of the figure illustrates evaporation behavior of a droplet that contains spheres, and the right-hand of the figure illustrates evaporation behavior of a droplet that contains ellipsoidal anisotropic particles. As shown in the figure, the presence of the anisotropic ellipsoids effects a uniform distribution of particles within the evaporated droplet.

[0126] Figure 22 illustrates the physical configuration of a droplet that is confined between two opposing plates. On the left-hand side of the figure is shown a standard droplet placed on a substrate, the droplet having an upper surface that is exposed to the environment exterior to the droplet. The right-hand side of figure illustrates a confined droplet, where the droplet is confined between upper and lower substrates. The confinement may act to impair the ability of ellipsoids (or other particles) from reaching the air-fluid interface.

[0127] The effects of the presence of anisotropic particles in a confined droplet are shown in Figure 23. As shown in that figure, ellipsoids are distributed more evenly than spheres upon evaporation of a confined droplet. The greater the aspect ratio, the more evenly the distribution of the particles following evaporation.

[0128] Figure 24 illustrates that in a droplet that contains spherical particles and ellipsoids (anisotropic particles), the spheres distribute more evenly upon evaporation than they do in a droplet that contains only spherical particles. As shown in the figure, the presence of anisotropic particles effects an essentially uniform distribution of spheres in a droplet following evaporation. In the exemplary embodiment shown in Figure 24, the volume fraction of spheres to ellipsoids was approximately 10. It should be understood that this exemplary volume:volume ratio is not a minimum or maximum, as post-evaporation uniform particle distribution may be achieved by other ratios of anisotropic particles to spheres.

ADDITIONAL DISCLOSURE

[0129] When colloidal particles adsorb onto air-water, oil-water, and other such interfaces, novel elastic membranes are created. The mechanical properties of these colloidal monolayer membranes (CMMs) may depend on many factors, including surface tension, capillary forces, particle size, shape, hydrophobicity, packing, and interaction potential. The

resulting interface phenomenology is rich with physics that influences a wide range of applications from film drying to Pickering emulsion stabilization.

[0130] Full understanding of the elastic character of these membranes remains elusive. Recently, progress has been made towards the measurement of the bulk, shear, and Young's moduli of CMMs and towards an understanding of particle-induced interfacial mechanisms. Effects due to particle shape, for example, can be qualitatively explained by shape-dependent capillary interactions; i.e., stiff membranes induced by ellipsoids at the air-water interface are more difficult to deform. One mechanical property of CMMs that has not as yet been measured is bending rigidity. Bending rigidity is of interest because the buckling behavior of membranes is controlled by the ratio of bending rigidity (κ) to Young's modulus (E), and the buckling behavior of membranes can substantially affect phenomena such as particle deposition during droplet evaporation.

[0131] Presented here are measurements of the bending rigidity of various colloidal monolayer membranes. Presented is a novel method for extracting bending properties of CMMs which employs evaporating drops in confined geometries and readily permits study of particle-shape effects. To this end, colloidal drops composed of particles with approximately the same chemical composition, but with shapes ranging from spheres to ellipsoids, are confined between two glass plates and left to evaporate [Fig. 27(a)]. During evaporation, the air-water interface is observed to buckle in a manner similar to spherical-shell shaped elastic membranes. To extract membrane bending rigidity, one may extend the analytic description of buckled spherical membranes to a quasi-two dimensional geometry. One may find that CMM bending rigidity increases with increasing adsorbed-particle shape anisotropy. Besides measurement of bending rigidity, its consequences on particle deposition during evaporation in confined geometries are explored. Increased interfacial bending rigidity dramatically changes particle deposition during evaporation. Spheres can locally pin the three-phase contact line, which then bends around the pinning site and produces an uneven deposition. Conversely, the large bending rigidity induced by adsorbed ellipsoids makes deformation of the contact line energetically costly and ultimately induces uniform deposition. Surprisingly, drops of spheres doped with small numbers of ellipsoids are also deposited relatively uniformly in these confined geometries.

[0132] The exemplary experiments presented here utilize micron-sized polystyrene particles with modified shape, stretched asymmetrically to different major-minor diameter aspect ratio, α. The spheres are 1.3 μm in diameter; all ellipsoids are stretched from these same 1.3 μm

spheres. The colloidal drops are confined between two glass slides separated by 38.1 μm spacers (Fisher Scientific); qualitatively similar results are found for chambers made from slightly hydrophobic cover slips. The evaporation of these drops was investigated, i.e., suspensions containing particles of the same composition but with different major-minor diameter aspect ratios, including spheres ($\alpha = 1.0$), slightly deformed spheres ($\alpha = 1.2, 1.5$), and ellipsoids ($\alpha = 2.5, 3.5$).

The exemplary embodiments examine the particle volume fraction $\phi = 0.01$. (Qualitatively similar results are found for volume fractions ranging from ϕ - 10^{-4} to 0.05.) At these low volume fractions, particles densely coat the air-water interface before buckling events occur. Confinement chambers are placed within an optical microscope wherein evaporation is observed at video rates at a variety of different magnifications. Sample temperature is controlled within 0:1 °C.

[0133] During evaporation, the air-water interface deforms and crumples [Figs. 27(b) and 27(c)]. The buckling behaviors exhibited by the ribbonlike CMMs in confined geometries may depend on the shape of the adsorbed particles, and the buckling events appear similar to those observed in spherical-shell elastic membranes. Before buckling events occur, particles are maximally packed near the three-phase contact line, regardless of particle shape. Further, because the volume fraction is relatively low, membranes may contain a monolayer of particles; i.e., buckling events occur before multilayerparticle membranes form. These buckling events occur in-plane; i.e., the curvature in the z direction does not change after the membrane buckles .

[0134] One may quantify the elastic properties of the air-water interface with adsorbed particles (i.e., the elastic properties of the CMMs). One may extend analytical descriptions of elastic membranes to a quasi-2D geometry wherein observations about bending and buckling geometry are unambiguous. Briefly, the bending energy ($\propto \kappa h\zeta^2/d^3$, where κ is the 2D bending rigidity) and stretching energy ($\propto E(\zeta/r)^2 dh$, where E is the 2D Young's modulus) associated with an in-plane buckling event are minimized with respect to the ''rim width'' of the deformation, d [Figs. 27(b)–27(d)]. Here, ς is the radial displacement of the membrane from its initial configuration, h is the chamber height, and r is the in-plane radius of the droplet. More specifically, d is the width of the rim formed by the bent air-water interface, where the deformation bending and stretching energy is concentrated. One may measure d as the rim full-width, 25 μm in from the rim vertex [defined in Figs. 27(b)–27(d)]. (Note, d is independent of

the depth of the invagination. Thus, measurements of d are unaffected by pinning events during buckling.)

[0135] This approach enables one to extract the ratio of the ribbonlike CMM bending rigidity, κ, to its Young's modulus, E, from measurements of d and r.. In particular, minimizing the bending and stretching energy with respect to d yields the relation $\kappa = E\, d^4 / (3r^2)$. With all other parameters constant, e.g., particle anisotropy, etc., this formula predicts that $d \propto \sqrt{r}$. (Note, this derivation assumes that the interfacial displacement varies little in the z direction; i.e., the air-water interface deflects the same distance at the top, middle, and bottom of the chamber.) In Fig. 27(e) is presented data from evaporated drops of particles with anisotropy $\alpha = 1.2$ and with different initial values of r, plotting d versus $\sqrt{r}$. A linear relationship is observed (coefficient of determination, $R^2 = 0.93$), implying that the analysis is self-consistent. Similar linear results were found for other values of α.

[0136] One may thus extract and plot κ / E for evaporating drops of particles with different α [Fig. 27(f)]. $\kappa = E$ increases with increasing α, implying that as α increases, κ increases faster than E; i.e., κ / E is larger for ellipsoids ($\alpha = 2.5$ and 3.5) than for spheres ($\alpha =$ 1.0). CMM Young's modulus is known to increase with α. Utilizing reported measurements and calculations of E, one may plot κ versus E [Fig. 27(g)] and find that $\kappa \propto E^{2.94(3)}$. This observation is consistent with theoretical models which predict $\kappa \propto E^3$. One may use measurements and calculations of E to isolate and estimate the ribbonlike CMM bending rigidity [Fig. 27(h)]. Membrane bending may become more difficult with increasing particle anisotropy.

[0137] One may also examine the consequences of increased bending rigidity on evaporation processes in confined geometries, specifically particle deposition during drying. Substantial effort has now yielded an understanding of the so-called coffee ring effect and some ability to control particle deposition from sessile drops. However, much less is known about particle deposition in confined geometries, despite the fact that many real systems and applications feature evaporation in geometries wherein the air-water interface is present only at the system edges. Recent experiments have explored evaporation of confined drops containing spheres, and their behaviors differ dramatically from sessile drops containing spheres. In the confined case, as noted previously, particles are pushed to the ribbonlike air-fluid interface, and, as evaporation proceeds, the particle-covered air-water interface often undergoes the buckling events described above.

[0138] One may find that suspended particle shape produces dramatically different depositions as a result of the varying CMM bending moduli. In Figs. 28(a)–2(e), the final deposition of particles is shown for $\alpha = 1.0, 1.2, 1.5, 2.5, 3.5$, respectively. Spheres and slightly stretched spheres are deposited heterogeneously, and anisotropic ellipsoids are distributed relatively more uniformly. To describe the final deposition of particles more quantitatively, one may plot the fraction of initial droplet area covered by deposited particles after drying, f, as a function of anisotropy α [Fig. 28(f)]. Note, for uniformly deposited particles, the area fraction (based on the initial volume fraction, initial volume, chamber height, and particle size) would be ~0:4; thus, regions with area fraction ≈ 0:4 are considered as covered. The fraction of the area covered with particles is observed to increase with α. For $\alpha = 1.2$ and 1.5, f increases modestly. For $\alpha = 2.5$, the deposition is very uniform, and for $\alpha = 3.5$, virtually the entire area is covered uniformly.

[0139] High magnification images reveal why spheres and slightly stretched particles deposit unevenly, while ellipsoids deposit more uniformly [Figs. 25(a)–25(d)]. Spheres and slightly stretched spheres often pin the air-water interface, preventing its motion. Spheres can pin the air-water interface even in very dilute suspensions, i.e., $\phi < 10^{-4}$. As evaporation continues, the CMM interface bends around the pinning site [Fig. 25(a)]. Then, it either pinches off, leaving particles behind, or it remains connected to the pinned site, leading to water flow into the narrow channel that has formed; the latter flow carries particles towards the pinning site [Fig. 25(a) and 25(b)] producing "streaks" of deposited particles [Fig. 25(c)]. Temporal and spatial heterogeneities along the interface due to these described effects lead to heterogeneous deposition of spherical particles during evaporation.

[0140] When ellipsoids approach the drop edge they also adsorb onto the air-water interface forming ribbonlike CMMs [Fig. 25(d)]. However, the ellipsoids induce substantial capillary deformations on the air-water interface, creating an elastic membrane with a high bending rigidity. Ellipsoids can also pin the contact line, but bending of the CMM interface around a pinned contact line requires an energetically costly rearrangement of ellipsoids aggregated on the CMM; i.e., attractive particle-particle capillary interactions are be overcome (even at very small ϕ). Conversely, bending of the contact line costs little energy to spheres on the interface because sphere-sphere capillary interactions on the interface are much weaker than for ellipsoids. As evaporation continues, the ellipsoid- CMM contact line recedes radially, and the ellipsoids near the contact line are deposited on the substrate. This behavior is similar to

convective assembly techniques wherein a drying front is created by pulling the substrate away from the contact line or by heating a confined drop near the contact line; in each case a thin film is thus formed that leads to the creation of a monolayer. The present system, by contrast, has neither moving nor mechanical parts. Uniform coatings are created essentially as a result of shape-induced capillary attractions which produce CMMs that are hard to bend.

[0141] To further elucidate the effects of particle shape on deposition, suspensions of 200 nm spheres ($\alpha = 1.0$) with $\phi = 0{:}02$ were combined with suspensions containing micron-sized ellipsoids ($\alpha = 3{:}5$) at lower volume fractions, $\phi = 0$ to $4{:}0 \times 10^{-3}$. The resulting colloidal drops were evaporated in the same confined geometries. The addition of a very small number of ellipsoids has no effect on the deposition of spheres ($\phi \leq 1.7 \times 10^{-3}$). Surprisingly, the addition of a larger, but still small, number of ellipsoids leads to a uniform deposition of both ellipsoids and spheres, i.e., $f \approx 0{:}8$, despite the fact that spheres outnumber ellipsoids by a significant factor (10^3–10^4) [Fig. 25(e)]. Apparently, spheres do not prevent ellipsoids from adsorbing on the air-water interface, and the CMM bending rigidity is dominated by the presence of ellipsoids. Thus, the membrane still resists bending around pinning sites. This behavior in confined geometries is different than that of sessile drops wherein it was discovered that if the spheres are larger than the ellipsoids, then the spheres are distributed uniformly after drying, but if the spheres are smaller than the ellipsoids, then they exhibit the coffee ring effect. It is thus surprising that small spheres are deposited uniformly from droplets doped with small numbers of ellipsoids and confined between glass plates.

[0142] Again, the high bending modulus produced by ellipsoids on the CMM helps explain the observations. Both spheres and ellipsoids attach to the air-water interface. Ellipsoids deform the air-water interface, creating an effective elastic membrane with a high bending rigidity. When enough ellipsoids are present, pinning and bending the interface becomes energetically costly and the spheres (and ellipsoids) are deposited as the interface recedes.

[0143] To summarize, ellipsoids adsorbed on the air-water interface create an effective elastic membrane, and, as particle anisotropy aspect ratio increases, the membrane's bending rigidity increases faster than its Young's modulus. As a result, when a drop of a colloidal suspension evaporates in a confined geometry, the different elastic properties produce particle depositions that are highly dependent on particle shape. This observed increase in bending rigidity with particle shape aspect ratio holds consequences for applications of colloidal

monolayer membranes as well. For example, increased bending rigidity may help stabilize interfaces (e.g., Pickering emulsions) and thus could be useful for industrial applications, e.g., food processing. In a different vein, the observations suggest that CMMs in confined geometries may be a convenient model system to study buckling processes that are relevant for other systems, e.g., polymeric membranes, biological membranes, and nanoparticle membranes.

[0144] The following references are incorporated herein in their entireties for all purposes.

1. Deegan, R. D. et al. Capillary flow as the cause of ring stains from dried liquid drops. Nature. 389, 827-829 (1997).

2. Denkov, N. D. et al. Two-dimensional crystallization. Nature. 361, 26 (1993).

3. Hu, H. & Larson, R. G. Evaporation of a Sessile Droplet on a Substrate. The Journal of Physical Chemistry B. 106, 1334-1344 (2002).

4. Deegan, R. D. et al. Contact line deposits in an evaporating drop. Physical Review E. 62, 756-765 (2000).

5. Deegan, R. D. Pattern formation in drying drops. Physical Review E. 61, 475-485 (2000).

6. Bigioni, T. P. et al. Kinetically driven self assembly of highly ordered nanoparticle monolayers. Nature Materials. 5, 265-270 (2006).

7. Kaya, D., Belyi, V. A. & Muthukumar, M. Pattern formation in drying droplets of polyelectrolyte and salt. The Journal of Chemical Physics. 133, 114905 (2010).

8. Park, J. & Moon, J. Control of Colloidal Particle Deposit Patterns within Picoliter Droplets Ejected by Ink-Jet Printing. Langmuir. 22, 3506-3513 (2006).

9. Dugas, V. Immobilization of single-stranded DNA fragments to solid surfaces and their repeatable specific hybridization: covalent binding or adsorption? Sensors and Actuators B: Chemical.101, 112-121 (2004).

10. Dugas, V., Broutin, J. & Souteyrand, E. Droplet Evaporation Study Applied to DNA Chip Manufacturing. Langmuir. 21, 9130-9136 (2005).

11. deGans, B. J., Duineveld, P. . C. & Schubert, U. . S. Inkjet Printing of Polymers: State of the Art and Future Developments. Advanced Materials. 16, 203-213 (2004).

12. Hu, H. & Larson, R. G. Marangoni Effect Reverses Coffee-Ring Depositions. The Journal of Physical Chemistry B. 110, 7090-7094 (2006).

13. Weon, B. M. & Je, J. H. Capillary force repels coffee-ring effect. Physical Review E. 82,015305 (2010).

14. Kajiya, T., Kobayashi,W., Okuzono, T. & Doi, M. Controlling the Drying and Film Formation Processes of Polymer Solution Droplets with Addition of Small Amount of Surfactants. The Journal of Physical Chemistry B. 113, 15460-15466 (2009).

15. Nguyen, V. X. & Stebe, K. J. Patterning of Small Particles by a Surfactant-Enhanced Marangoni-Benard Instability. Physical Review Letters. 88, 164501 (2002).

16. Park, B. J. & Furst, E. M. Fluid-interface templating of two-dimensional colloidal crystals. Soft Matter. 6, 485-488 (2010).

17. Loudet, J. C., Yodh, A. G. & Pouligny, B. Wetting and Contact Lines of Micrometer-Sized Ellipsoids. Physical Review Letters. 97, 018304 (2006).

18. Loudet, J. C., Alsayed, A. M., Zhang, J. & Yodh, A. G. Capillary Interactions Between Anisotropic Colloidal Particles. Physical Review Letters. 94, 018301 (2005).

19. Bowden, N., Arias, F., Deng, T. & Whitesides, G. M. Self-Assembly of Microscale Objects at a Liquid/Liquid Interface through Lateral Capillary Forces. Langmuir. 17, 1757-1765 (2001).

20. Brown, A. B. D., Smith, C. G. & Rennie, A. R. Fabricating colloidal particles with photolithography and their interactions at an air-water interface. Physical Review E. 62, 951-960 (2000).

21. Madivala, B., Fransaer, J. & Vermant, J. Self-Assembly and Rheology of Ellipsoidal Particles at Interfaces. Langmuir. 25, 2718-2728 (2009).

22. Madivala, B., Vandebril, S., Fransaer, J. & Vermant, J. Exploiting particle shape in solid stabilized emulsions. Soft Matter. 5, 1717-1727 (2009).

23. Park, B. J. & Furst, E. M. Attractive interactions between colloids at the oil-water interface. Soft Matter. (2011)

24. Fournier, J. B. & Galatola, P. Anisotropic capillary interactions and jamming of colloidal particles trapped at a liquid-fluid interface. Physical Review E. 65, 031601 (2002).

25. Champion, J. A., Katare, Y. K. & Mitragotri, S. Making polymeric micro- and nanoparticles of complex shapes. Proceedings of the National Academy of Sciences. 104, 11901-11904 (2007).

26. Ho, C. C., Keller, A., Odell, J. A. & Ottewill, R. H. Preparation of monodisperse ellipsoidal polystyrene particles. Colloid and Polymer Science. 271, 469-479 (1993).

27. Lehle, H., Noruzifar, E. & Oettel, M. Ellipsoidal particles at fluid interfaces. The European Physical Journal E: Soft Matter and Biological Physics. 26, 151-160 (2008).

28. Lewandowski, E. P., Bernate, J. A., Tseng, A., Searson, P. C. & Stebe, K. J. Oriented assembly of anisotropic particles by capillary interactions. Soft Matter. 5, 886-890 (2009).

29. Danov, K. D. & Kralchevsky, P. A. Capillary forces between particles at a liquid interface: General theoretical approach and interactions between capillary multipoles. Advances in Colloid and Interface Science. 154, 91-103 (2010).

30. Stamou, D., Duschl, C. & Johannsmann, D. Long-range attraction between colloidal spheres at the air-water interface: The consequence of an irregular meniscus. Physical Review E. 62, 5263-5272 (2000).

31. Deegan, R. D. Pattern formation in drying drops. Physical Review E. 475–485 (2000).

32. H. A. Fluid motion of monomolecular films in a channel flow geometry. Physics of Fluids. 2931–2937 (1995).

33. P.J. Yunker, M. Gratale, M.A. Lohr, T. Still, T.C. Lubensky, and A.G. Yodh, Phys. Rev. Lett. 108, 228303 (2012)).

What is Claimed:

1. A method of creating an essentially uniform particle deposition, comprising:

applying, to a portion of a substrate, a composition comprising a fluid medium having a plurality of anisotropic bodies disposed within,

at least some of the anisotropic bodies having an aspect ratio of major axis to minor axis of between about 1.0 and about 10,000; and

evaporating at least a portion of the fluid medium,

the resulting evaporation producing a first essentially uniform deposition of particles across the portion of the substrate.

2. The method of claim 1, further comprising heating the deposited particles so as to fuse two or more particles to one another.

3. The method of 2, wherein the heating gives rise to a cohesive coating.

4. The method of claim 1, further comprising chemically treating the deposited particles so as to fuse two or more particles to one another.

5. The method of claim 4, wherein the chemical treatment gives rise to cohesive coating.

6. The method of claim 1, wherein the evaporation is performed under heating.

7. The method of claim 1, wherein the evaporation is performed under reduced humidity.

8. The method of claim 1, wherein the plurality of anisotropic bodies represents a volume fraction of from about 0.0001 to about 0.2 of the composition.

9. The method of claim 8, wherein the plurality of anisotropic bodies represents a volume fraction of from about 0.001 to about 0.02 of the composition.

10. The method of claim 1, wherein the fluid medium comprises water, alcohol, a hydrocarbon, or any combination thereof.

11. The method of claim 1, wherein the composition further comprises a population of essentially spherical bodies.

12. The method of claim 11, wherein at least a portion of the essentially spherical bodies have a diameter that is greater than the minor axis of the plurality of anisotropic bodies.

13. The method of claim 11, wherein one or more spherical bodies comprises a pigment.

14. The method of claim 11, wherein an essentially spherical body comprises a polymer, a biological entity, or both.

15. The method of claim 1, wherein an anisotropic body comprise a polymer, biological entity, a metal, or any combination thereof.

16. The method of claim 15, wherein an anisotropic body comprises a biological entity.

17. The method of claim 16, wherein a biological entity comprises a virus, a bacterium, a filament, or any combination thereof.

18. The method of claim 1, wherein the anisotropic bodies are characterized as being elliptical.

19. The method of claim 1, wherein the anisotropic bodies are characterized as being rod-shaped.

20. The method of claim 1, wherein the composition further comprises a pigment.

21. The method of claim 20, wherein one or more anisotropic bodies comprises a pigment.

22. The method of claim 20, wherein the composition comprises one or more pigment bodies having a major axis larger than the minor axis of the plurality of anisotropic bodies.

23. The method of claim 1, wherein at least some of the anisotropic bodies have an aspect ratio of major axis to minor axis of between about 10 and about 1,000.

24. The method of claim 23, wherein at least some of the anisotropic bodies have an aspect ratio of major axis to minor axis of between about 100 and about 500.

25. The method of claim 1, wherein the composition is disposed between two surfaces.

26. The method of claim 25, wherein the composition further comprises a population of essentially spherical bodies.

27. The method of claim 26, wherein at least a portion of the essentially spherical bodies have a diameter that is larger than the minor axis of the plurality of anisotropic bodies.

28. The method of claim 27, wherein one or more spherical bodies comprises a pigment.

29. The method of claim 28, wherein a spherical body comprises a polymer, a biological entity, or both.

30.c The method of claim 29, wherein a spherical body comprises a strand of DNA.

31. The method of claim 29, wherein a spherical body comprises an individual molecule.

32. The method of claim 1, further comprising disposing a second quantity of the composition atop the first essentially uniform deposition of particles across the portion of the substrate, and evaporating the fluid medium of the second quantity so as to deposit an essentially uniform deposition of particles atop the first essentially uniform deposition of particles.

33. A method of forming a composition for creating essentially uniform particle distributions, comprising:

dispersing a plurality of anisotropic bodies and a plurality of spherical bodies into a fluid medium,

at least some of the anisotropic bodies having an aspect ratio of major axis to minor axis of greater than about 1.0, and

the anisotropic bodies having at least one cross-sectional dimension in the range of between about 1.0 and about 10,000.

34. A method of forming a composition for creating essentially uniform particle distributions, comprising:

dispersing a plurality of anisotropic bodies into a fluid that contains a plurality of spherical bodies,

at least some of the anisotropic bodies having a aspect ratio of major axis to minor axis of greater than about 1.0, and

the anisotropic bodies having at least one cross-sectional dimension in the range of between about 1.0 and about 10,000.

35. The method of claim 34, wherein the fluid is characterized as an ink, a paint, or both.

36. A composition, comprising:

a fluid medium;

a plurality of anisotropic bodies disposed within the fluid medium,

at least some of the anisotropic bodies having hydrophobicities that differ from one another.

37. A composition, comprising:

a fluid medium;

a plurality of anisotropic bodies disposed within the fluid medium,

at least some of the anisotropic bodies having an aspect ratio of major axis to minor axis of between about 1.0 and about 10,000, and

at least some of the anisotropic bodies having at least one cross-sectional dimension in the range of from about 1 nm to about 500 micrometers.

38. The composition of claim 37, wherein the plurality of anisotropic bodies represents a volume fraction of from about 0.0001 to about 0.2 of the composition.

39. The composition of claim 38, wherein the plurality of anisotropic bodies represents a volume fraction of from about 0.001 to about 0.02 of the composition.

40. The composition of claim 37, wherein the fluid medium comprises water, alcohol, a hydrocarbon, or any combination thereof.

41. The composition of claim 37, further comprising a population of essentially spherical bodies.

42. The composition of claim 41, wherein at least a portion of the essentially spherical bodies have a diameter that is greater than the minor axis of the plurality of anisotropic bodies.

43. The composition of claim 41, wherein a spherical body comprises a polymer, a biological entity, or both.

44. The composition of claim 37, wherein an anisotropic body comprise a polymer, biological entity, a metal, or any combination thereof.

45. The composition of claim 37, wherein an anisotropic body comprises a biological entity.

46. The composition of claim 45, wherein a biological entity comprises a virus, a bacterium, a filament, or any combination thereof.

47. The composition of claim 37, wherein the anisotropic bodies are characterized as being elliptical.

48. The composition of claim 37, wherein the anisotropic bodies are characterized as being rod-shaped.

49. The composition of claim 37, further comprising a pigment.

50. The composition of claim 49, wherein one or more anisotropic bodies comprises a pigment.

51. The composition of claim 49, further comprising one or more pigment bodies having a major axis larger than the minor axis of the plurality of anisotropic bodies.

52. The composition of claim 37, wherein at least some of the anisotropic bodies having an aspect ratio of major axis to minor axis of between about 10 and about 1,000.

53. The composition of claim 37, wherein at least some of the anisotropic bodies having an aspect ratio of major axis to minor axis of between about 100 and about 500.

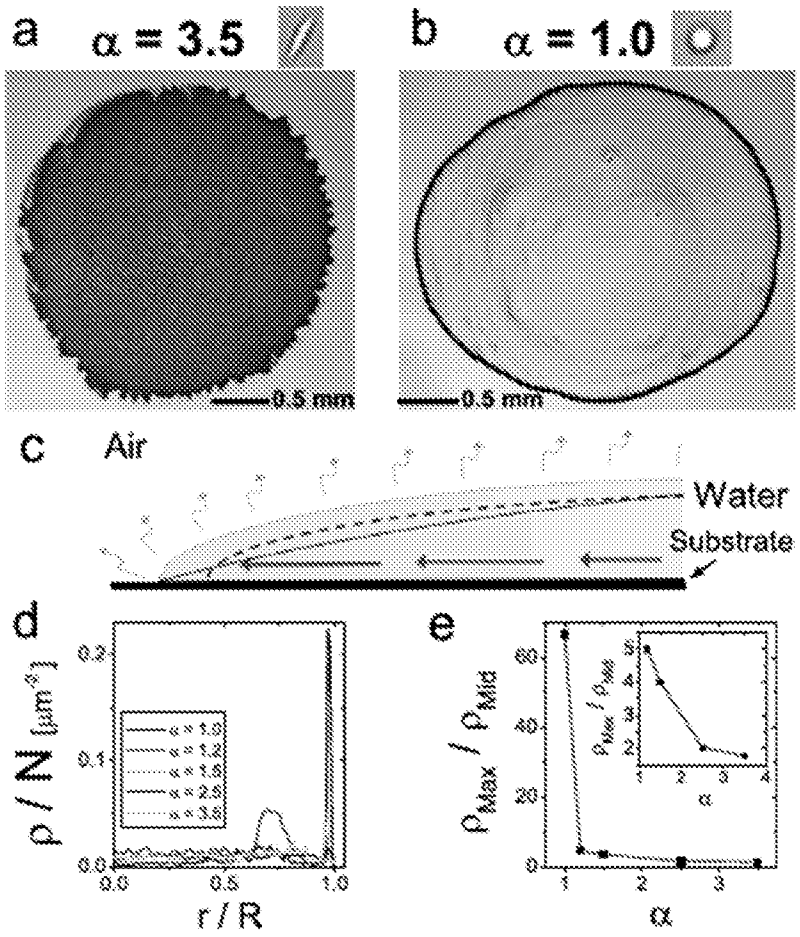
a
α = 3.5
b
α = 1.0
0.5 mm
0.5 mm
c
Air
Water
Substrate
d
ρ / N [μm⁻²]
r / R
e
ρMax / ρMid
α

Figure 1

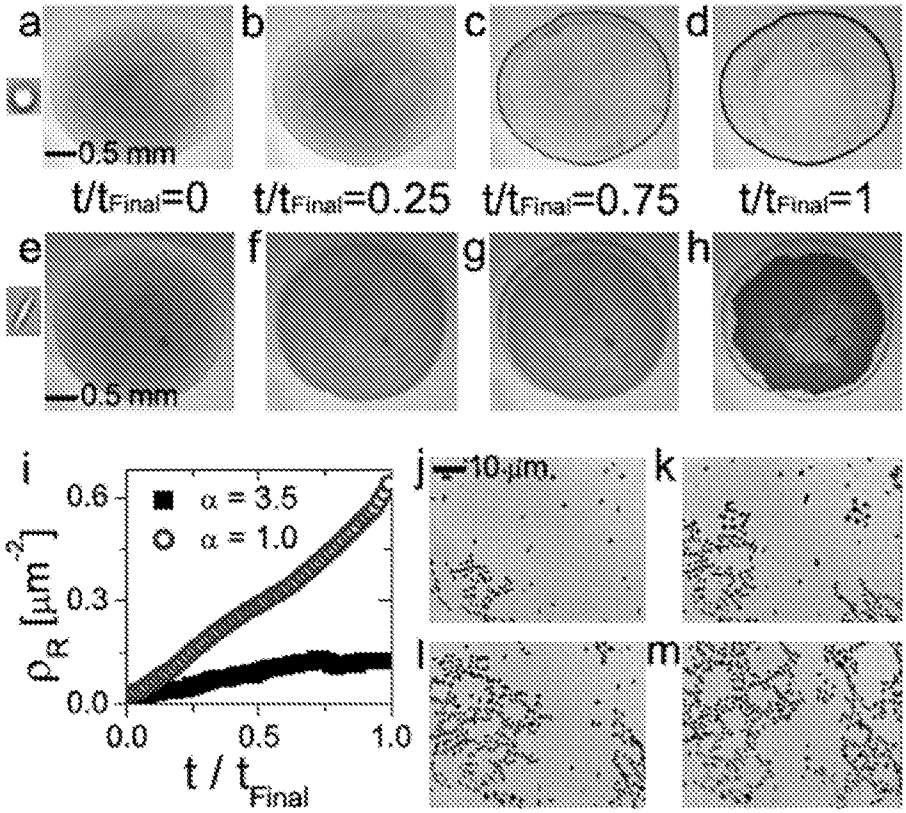
a
b
c
d
0.5 mm
t/t_Final=0
t/t_Final=0.25
t/t_Final=0.75
t/t_Final=1
e
f
g
h
0.5 mm
i
α = 3.5
α = 1.0
ρ_R [μm^-2]
0.6
0.3
0.0
0.0
0.5
1.0
t / t_Final
j
10 μm
k
l
m

Figure 2

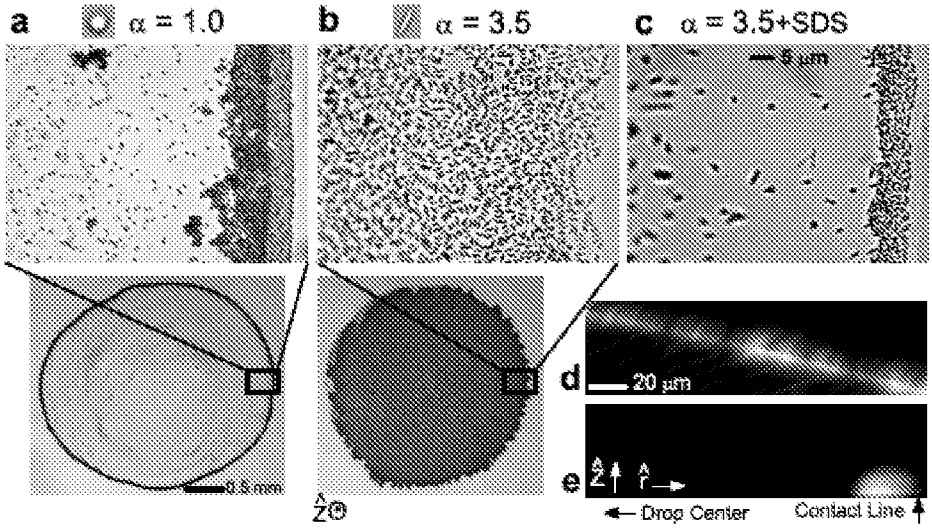

Figure 3

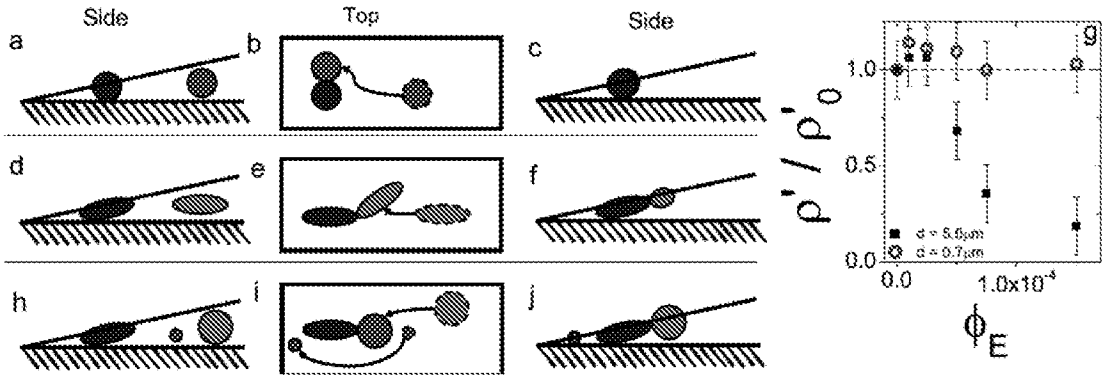

Figure 4

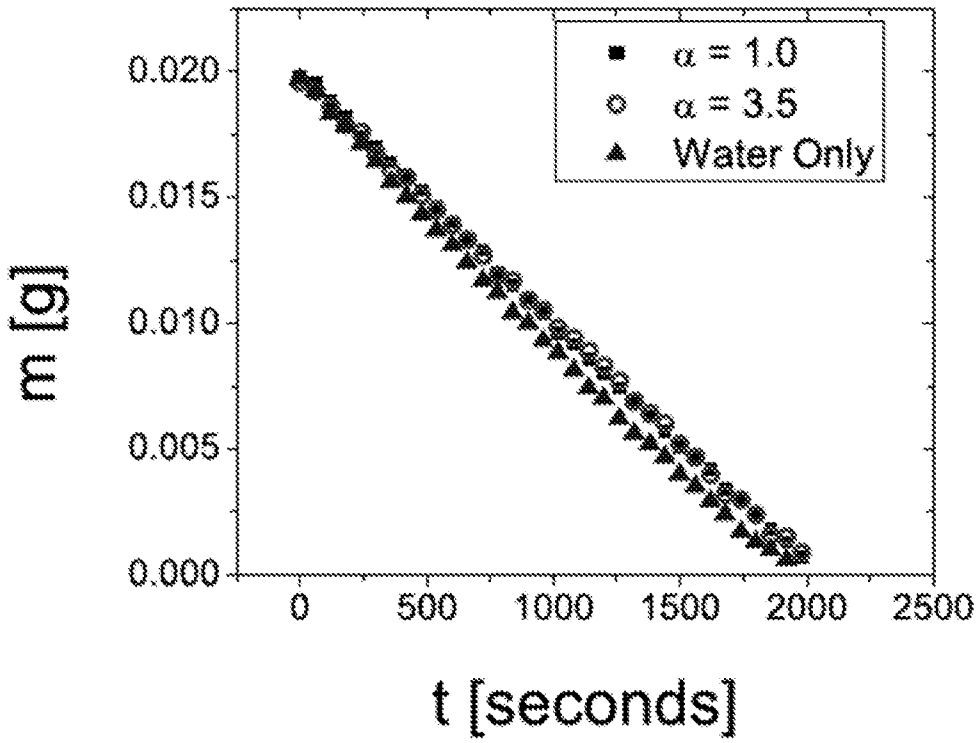
α = 1.0
α = 3.5
Water Only
0.020
0.015
0.010
0.005
0.000
m [g]
0
500
1000
1500
2000
2500
t [seconds]

Figure 5

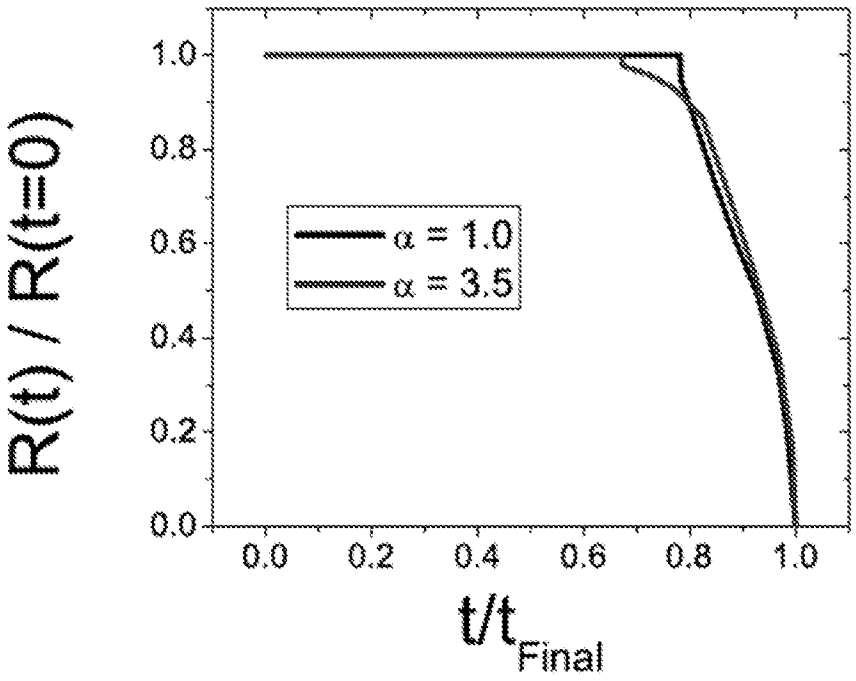

Figure 6

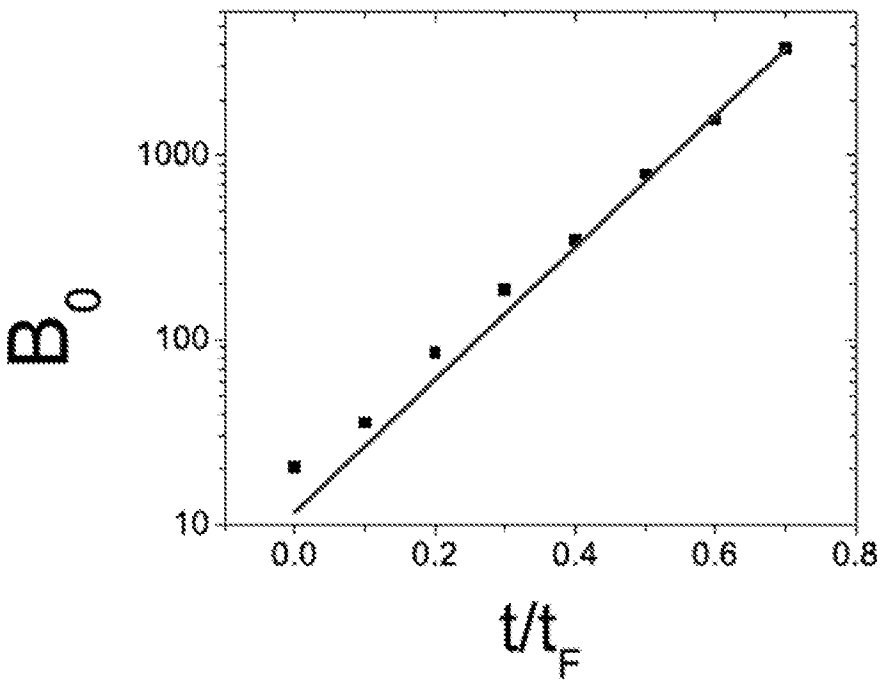

Figure 7

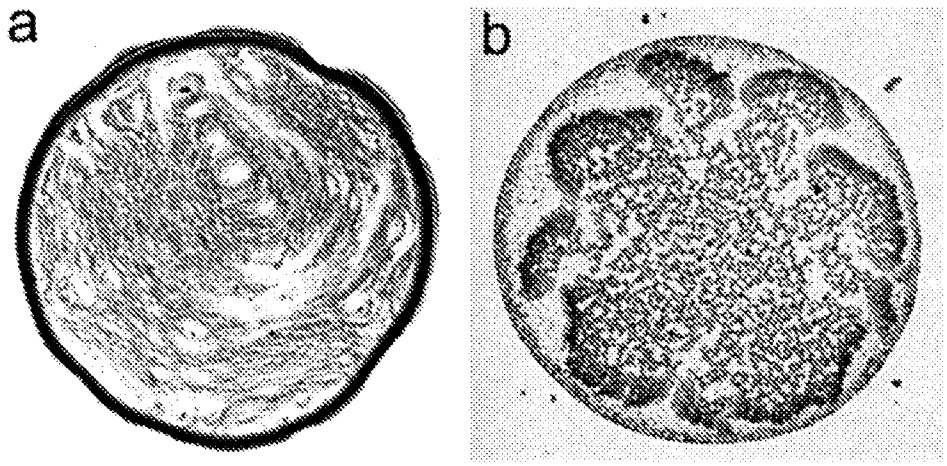

Figure 8

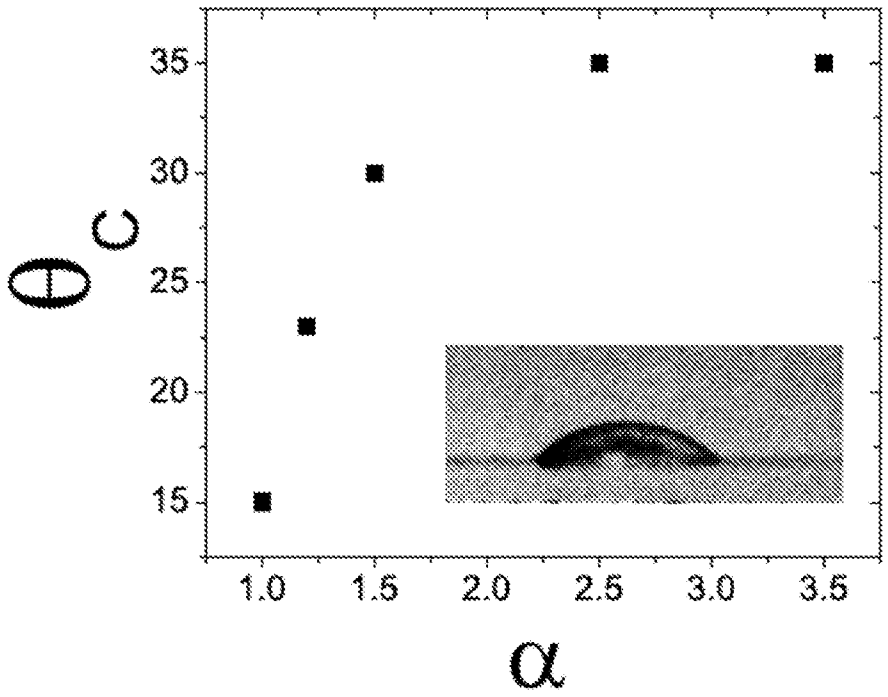

Figure 9

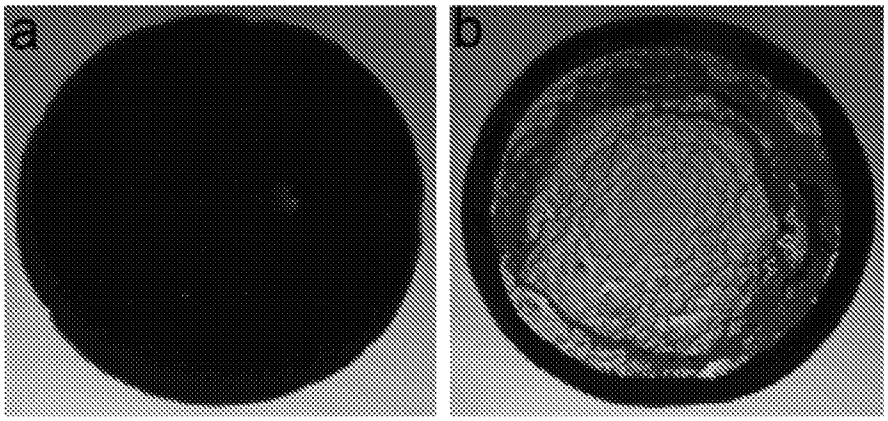

Figure 10

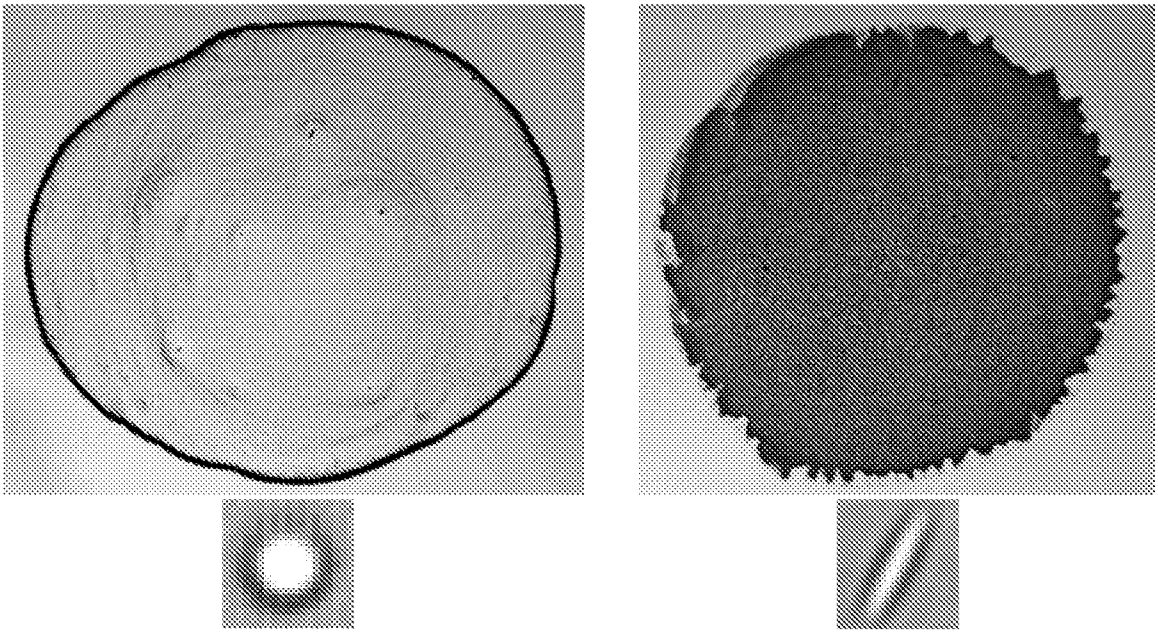

Figure 11

Figure 12

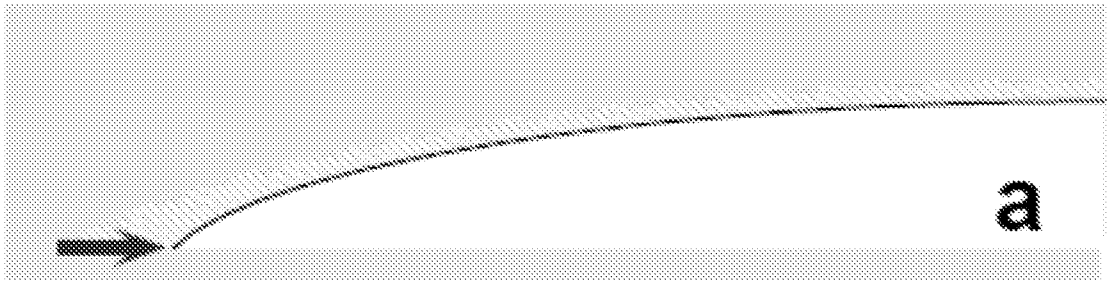

Figure 13

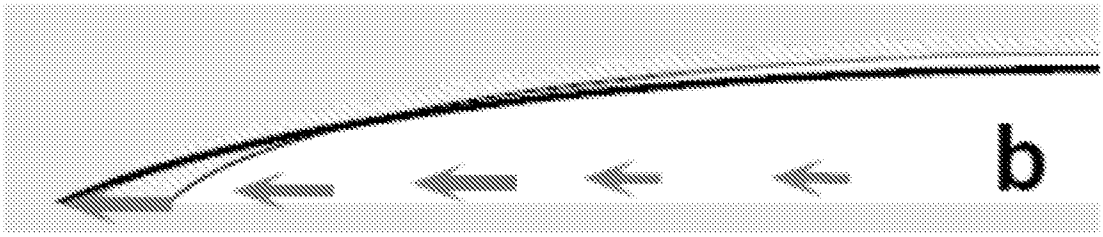

Figure 14

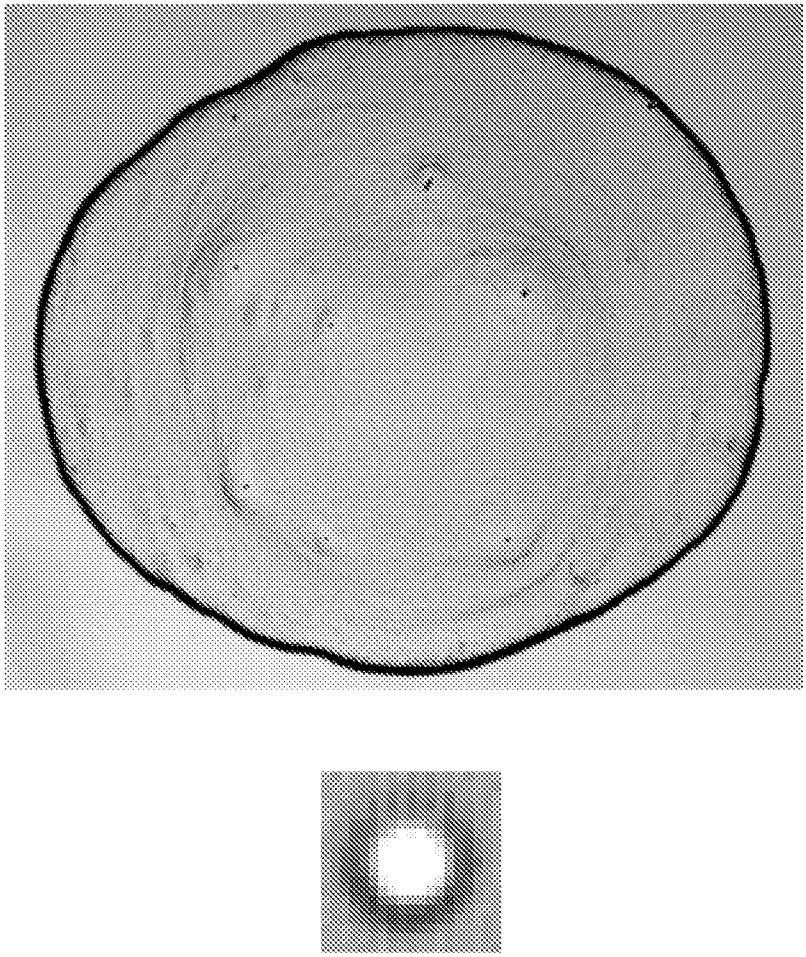

Figure 15

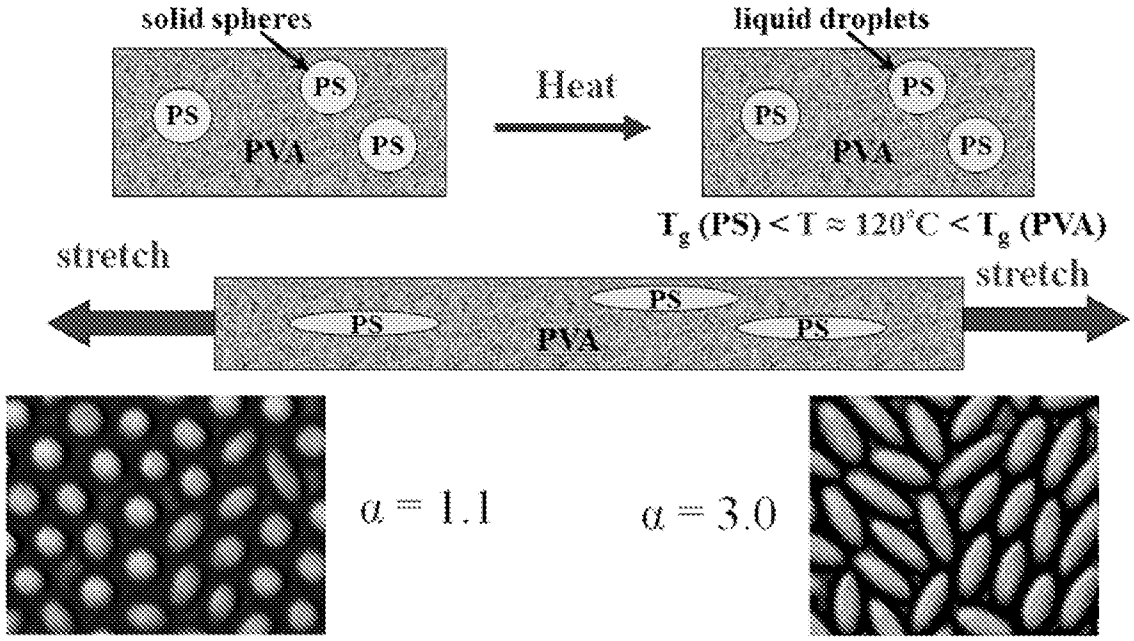
solid spheres
PS
PS
PS
PVA
Heat
liquid droplets
PS
PS
PS
PVA
T_g (PS) < T ≈ 120°C < T_g (PVA)
stretch
stretch
PS
PS
PS
PVA
α = 1.1
α = 3.0

Figure 16

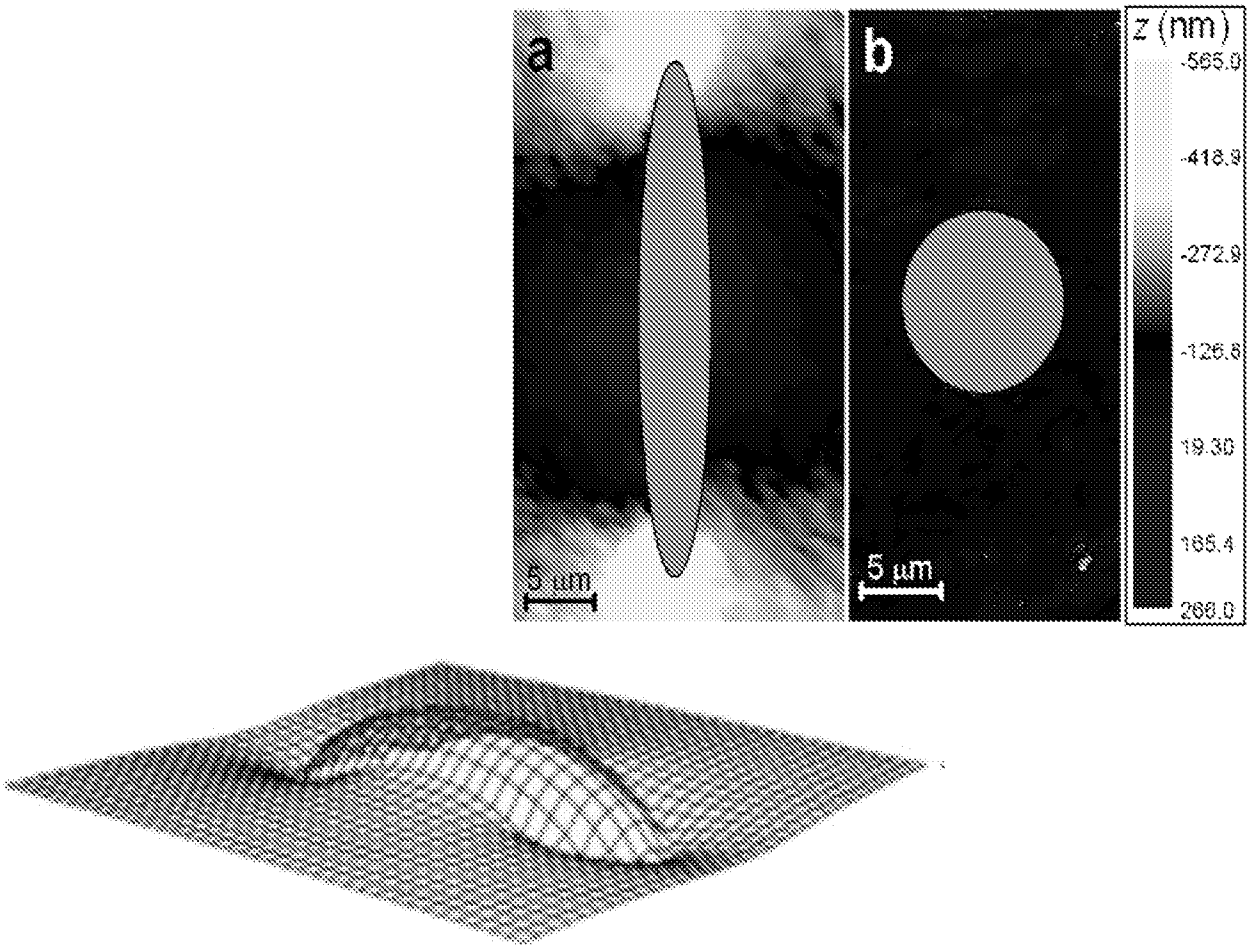

Figure 17

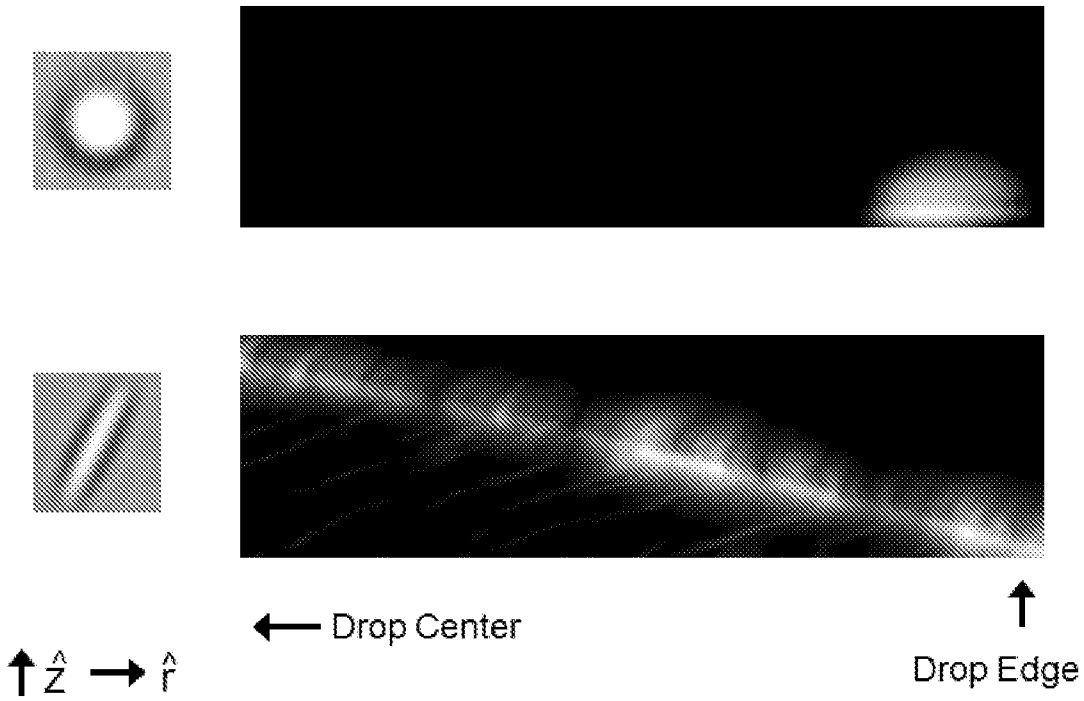

Figure 18

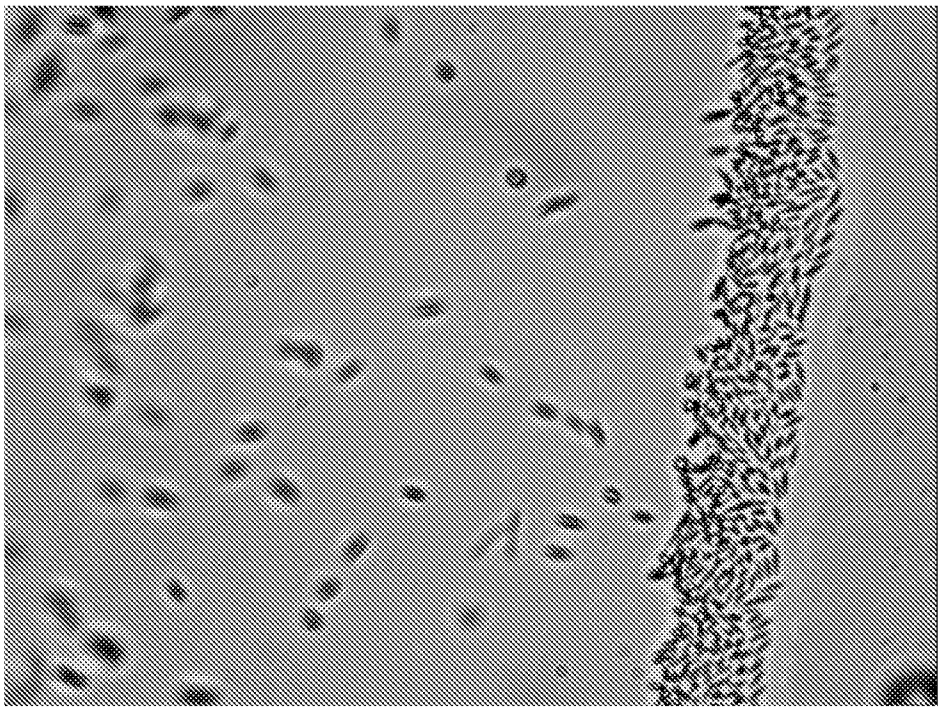

Figure 19

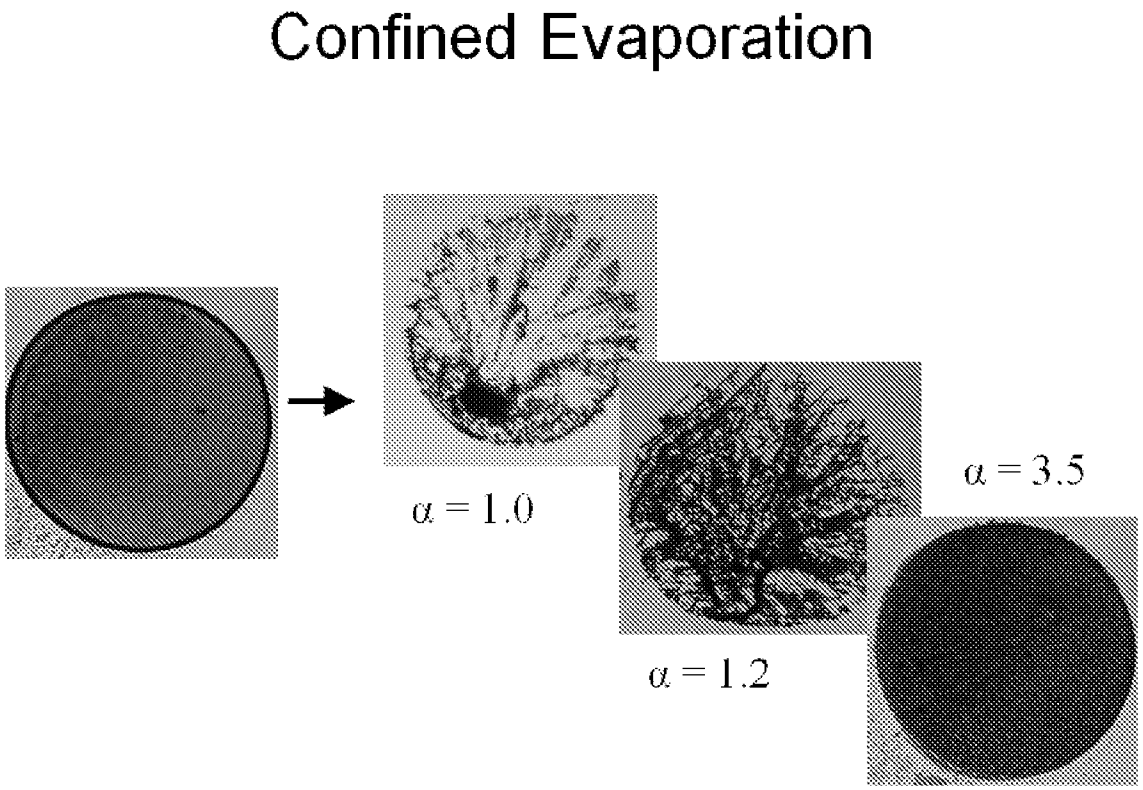

Figure 20

Ellipsoids Prevent the Coffee Ring Effect (Open/Sessile Drop)

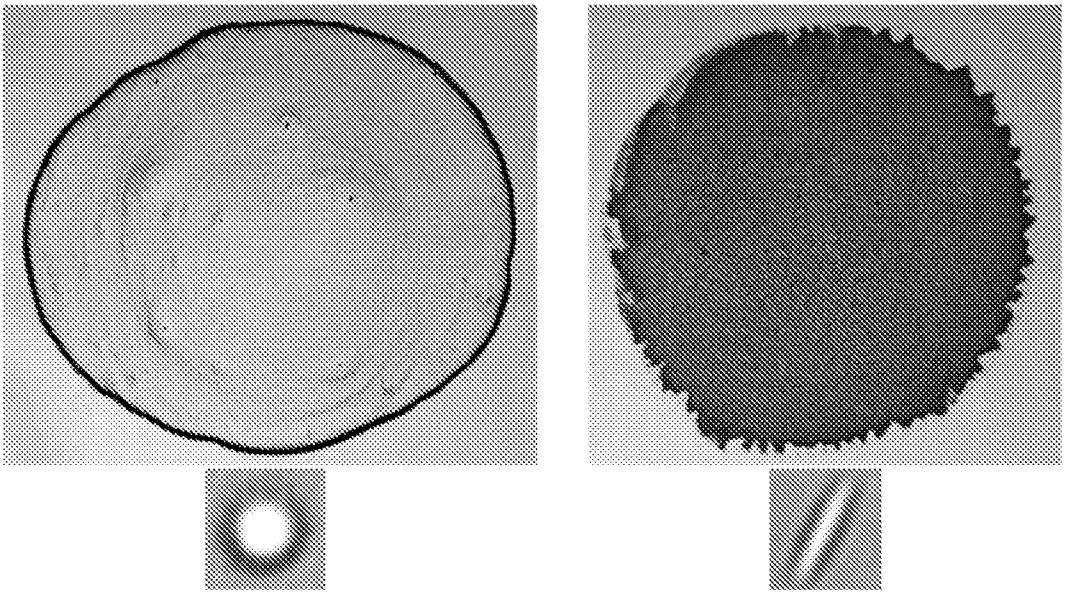

Figure 21

What about confined drops?

- Ellipsoids are carried to drop edge just like spheres
- Large air-water interface prevents ellipsoids from reaching edge
- What happens if interface is removed via confinement?

Figure 22

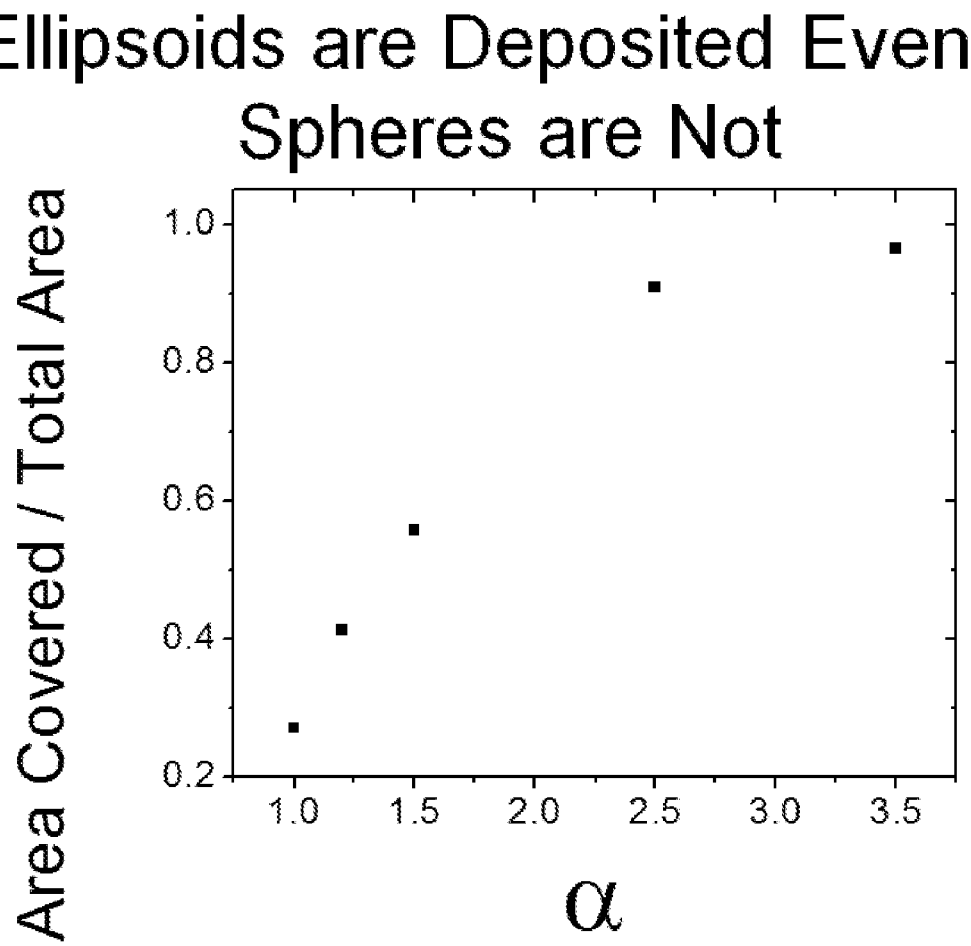
Ellipsoids are Deposited Evenly, Spheres are Not
Area Covered / Total Area
1.0
0.8
0.6
0.4
0.2
1.0
1.5
2.0
2.5
3.0
3.5
α

Figure 23

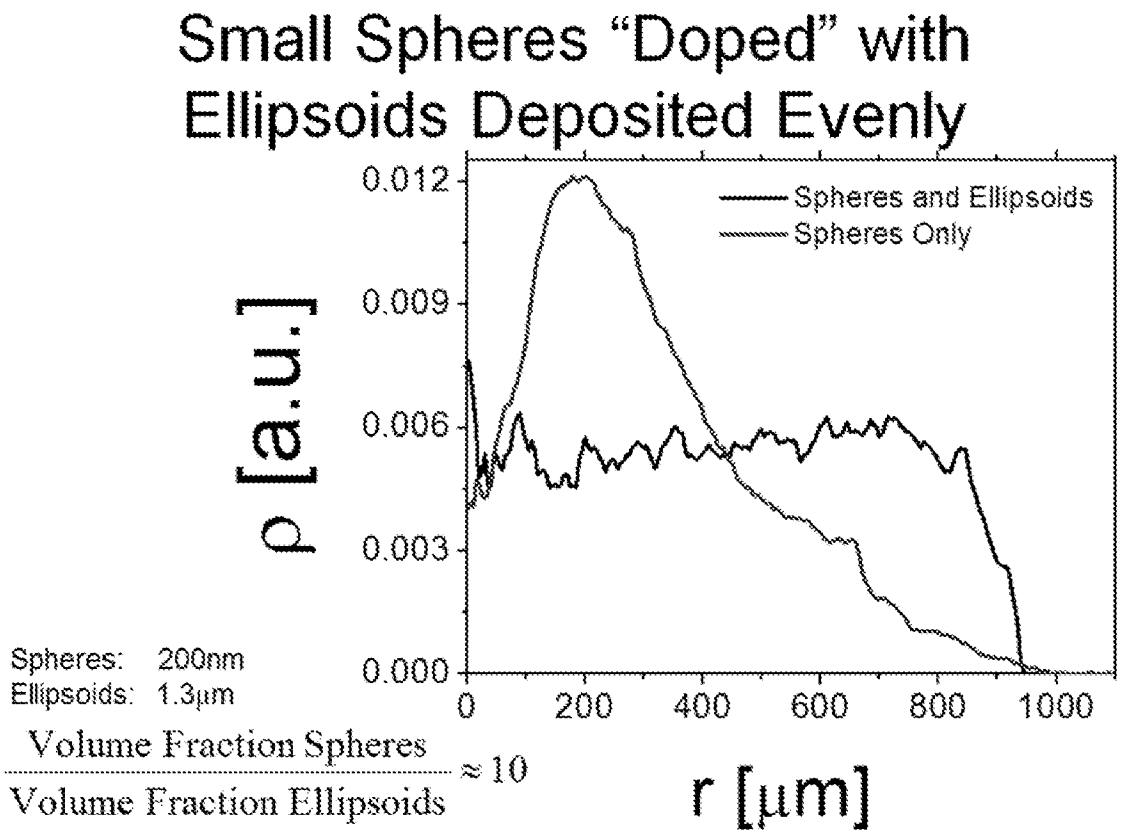
Small Spheres "Doped" with Ellipsoids Deposited Evenly
Spheres and Ellipsoids
Spheres Only
ρ [a.u.]
0.012
0.009
0.006
0.003
0.000
0
200
400
600
800
1000
r [μm]
Spheres: 200nm
Ellipsoids: 1.3μm
Volume Fraction Spheres / Volume Fraction Ellipsoids ≈ 10

Figure 24

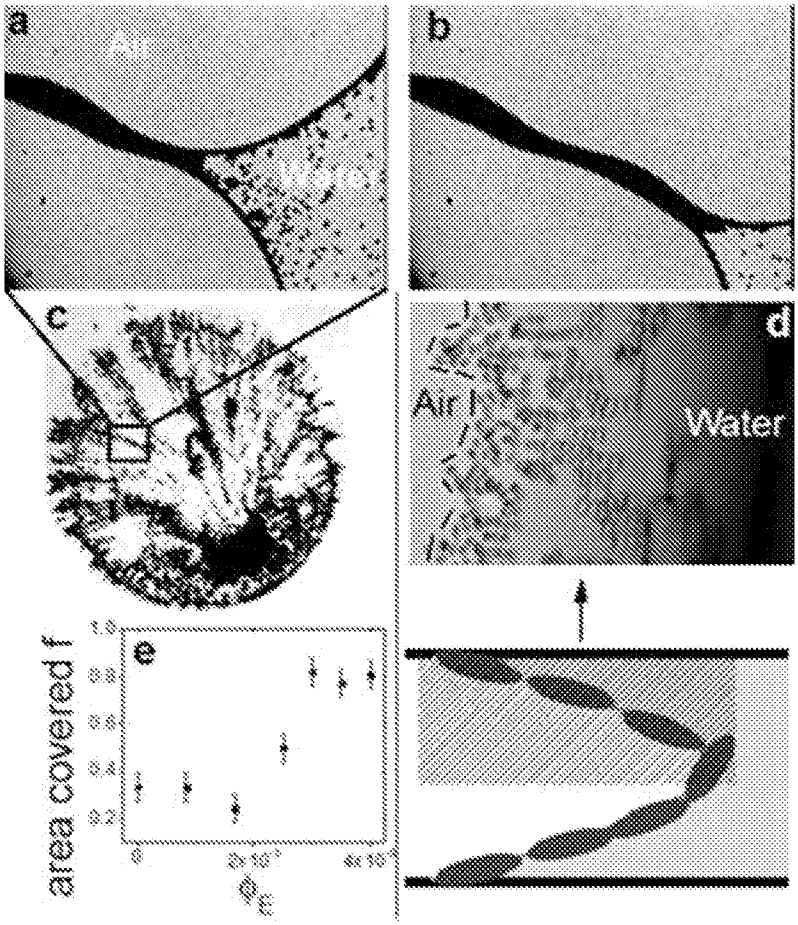
a
Air
Water
b
c
d
Air
Water
e
area covered f
1.0
0.8
0.6
0.4
0.2
0
2x10⁻⁷
4x10⁻⁷
Φ_E

Figure 25

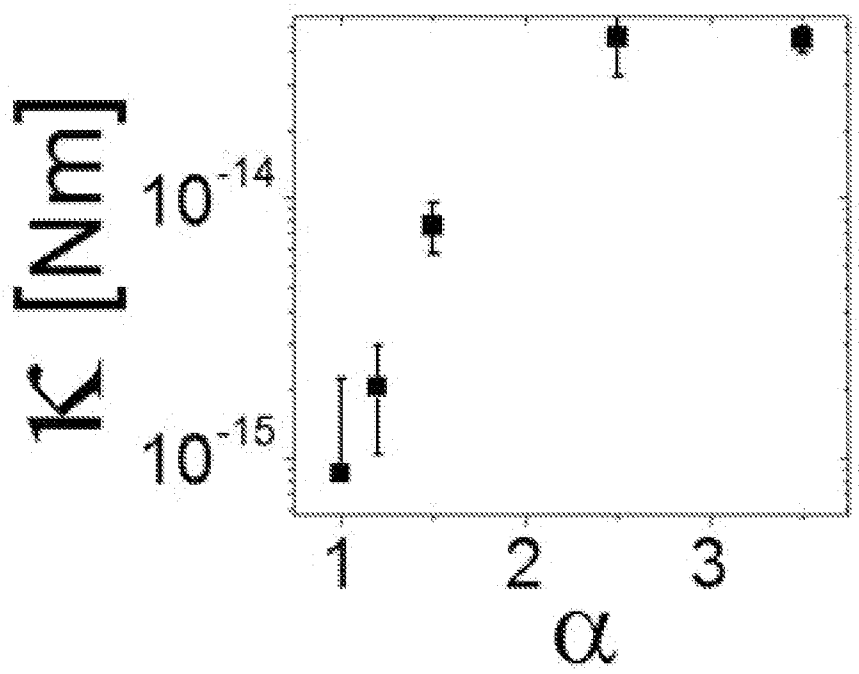

Figure 26

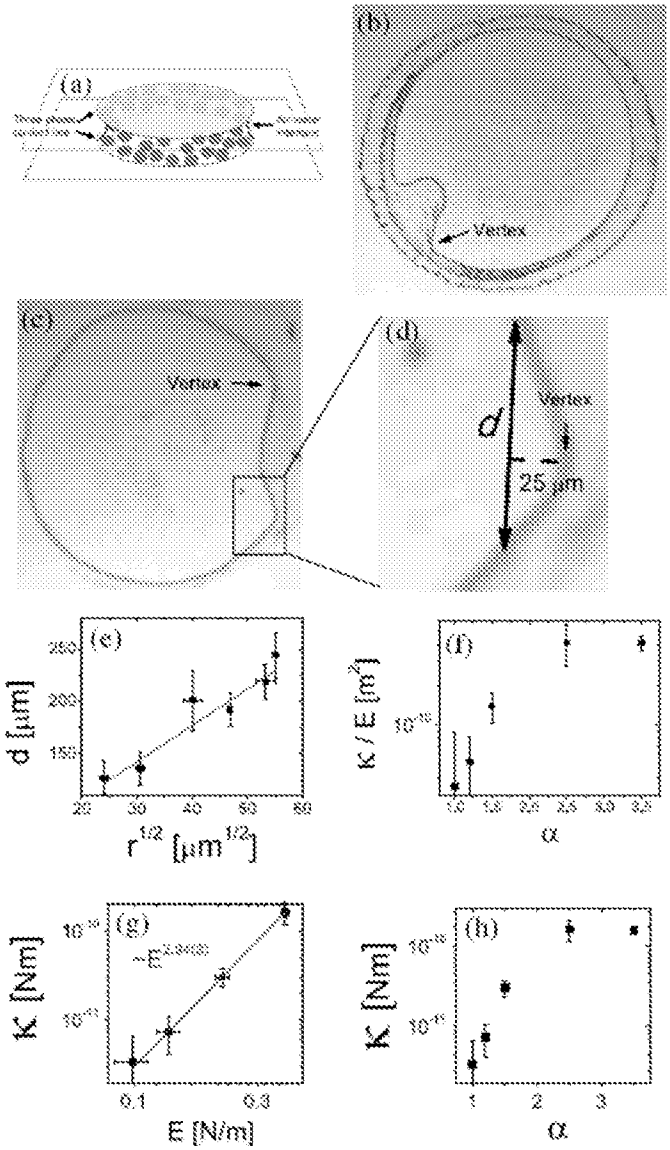
(a)
(b)
Vertex
(c)
Vertex
(d)
d
Vertex
25 μm
(e)
d [μm]
r^1/2 [μm^1/2]
(f)
κ / E [m^2]
α
(g)
κ [Nm]
E [N/m]
(h)
κ [Nm]
α

Figure 27

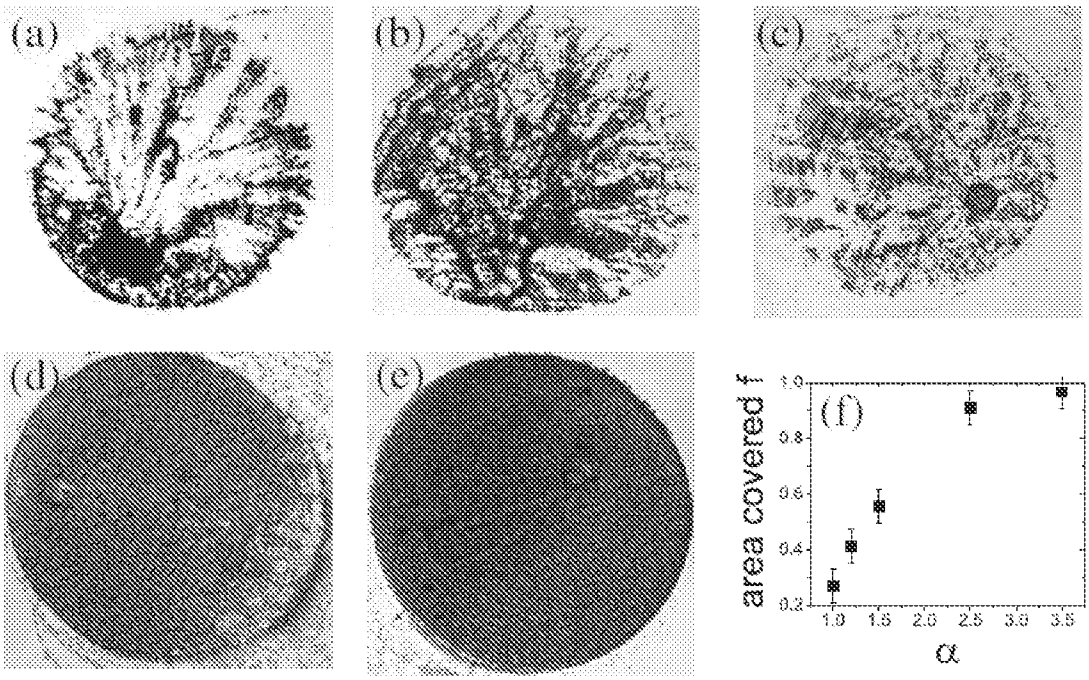

Figure 28